

Microbial symbionts buffer hosts against environmental variance in stochastic environments

Joshua C. Fowler,^{1*} Shaun Ziegler,² Kenneth D. Whitney,²
Jennifer A. Rudgers,² Tom E. X. Miller¹

¹Rice University, Department of BioSciences, Houston, TX, 77005

²University of New Mexico, Department of Biology, Albuquerque, NM, 87131

*To whom correspondence should be addressed; E-mail: jcf3@rice.edu.

ABSTRACT: The ability to cope with the negative consequences of environmental stochasticity will be critical to species' persistence in increasingly variable future climates. Yet, the role that microbial symbionts can play in buffering their hosts against variance has never been examined, despite the fact that practically all organisms host microbes. We document for the first time the role that *Epichloë* fungal symbionts of grasses plays in buffering variance through the analysis of a 14 year experiment manipulating the presence/absence of the symbiont in seven grass host species. Under the observed climate regime, this novel mechanism of mutualism provides contributions to fitness of the same magnitude as mean effects. In more variable climate scenarios, variance buffering takes on increased importance and leads to a strengthening of mutualism¹.

¹The abstract is limited to 125 words.

One sentence summary suggestions:

We need suggestions different from the title, please!

Main Text

Global climate change is driving increases in the variability of precipitation patterns and the frequency of extreme weather events (1–3). The consequences of this increased variability have received less attention than effects on mean climate conditions. Incorporating variability into forecasts of population dynamics is a key step towards improved predictions of the future. Classic theory predicts that long-term population growth rates (equivalently, population mean fitness) will decline under increased environmental variability due to negative effects of bad years that outweigh the positive effects of good years (a consequence of nonlinear averaging) (4, 5). For example, in unstructured populations, the long-term stochastic growth rate in fluctuating environments (λ_s) will always be smaller than the growth rate averaged across environments ($\bar{\lambda}$) by an amount proportional to the environmental variance (σ^2):

$$\log(\lambda_s) \approx \log(\bar{\lambda}) - \frac{\sigma^2}{2\bar{\lambda}^2} \quad (1)$$

Populations structured by size or stage similarly experience costs of variability (6, 7). Thus, there are two pathways to increase population viability in a stochastic environment: increase the mean growth rate ($\bar{\lambda}$) and/or dampen temporal fluctuation in growth rates, also called variance “buffering”.

Both the characteristics of species and the properties of environmental variability can buffer demographic fluctuations, including life history traits such as longevity (8, 9), correlations among vital rates (10), transient shifts in age/stage structure (11), the magnitude of environmental variability (12), or the degree of environmental autocorrelation (13, 14). These characteristics determine the risks of population extinction faced by species (15) and underlie conser-

vation management strategies promoting ecosystem resilience (16). Yet little is known about how biotic interactions alter demographic variability (17).

Most multicellular organisms host symbiotic microbes that impact growth and performance (18, 19), and many of these are transmitted via reproduction from maternal hosts to offspring (20). The process of vertical transmission links the fitness of hosts and symbionts together. This feedback selects for mutual benefits between host and symbiont, as anything less should cause them to go extinct within the population (21, 22). Many of these microbes have been observed to be mutualistic and protect hosts from environmental stresses including drought, extreme temperatures, or natural enemies (23–27). However, these protective mutualisms are context-dependent: the magnitude of benefits depends on environmental conditions (28) and thus will vary temporally in a stochastic environment (29, 30). Context-dependent benefits from symbionts may buffer hosts against variability through strong benefits during harsh periods, and neutral or even costly outcomes in benign periods, reducing the impacts of host exposure to extremes relative to non-symbiotic hosts. Variance buffering is a previously unexplored mechanisms by which symbionts may act as mutualists to their hosts, in addition to elevating average fitness, which may come to be of increasing importance in a more variable future (31)

We tested the hypothesis that context-dependent benefits of symbiosis buffer hosts from the fitness consequences of environmental variability using data from a unique, long-term symbiont-removal experiment in the field. We (i) quantified the effects of symbiosis on the mean and variance of host vital rates (survival, growth and reproduction), (ii) evaluated the relative contribution of mean and variance effects on long-term population growth rates, (iii) projected the consequences of variance buffering to population growth under increased variability using simulations, and (iv) investigated the relationship between host life history and symbiont-mediated variance buffering.

Initiated in 2007 in south-central Indiana, USA with seven grass species that host *Epichloë*

fungal endophytes, the experiment consisted of annually censused plots planted with either naturally symbiotic plants (S+) or those which have had their symbionts experimentally removed via a heat treatment (S-) (See SM for a full list of species and experimental methods). *Epichloë* fungi are specialized symbionts growing intercellularly in the aboveground tissue of ~ 30% of cool-season (C3) grass species (32). The fungi are primarily transmitted vertically from maternal plants through seeds (33, 34). They produce a variety of alkaloids that can protect host plants from herbivory (35) and drought stress (36–38).

The unique data from this long-term experiment are distinctly suitable for detecting fitness benefits of microbial symbiosis that arise through variance buffering. We collected annual demographic data on the vital rates (survival, growth, and reproduction) of all individual plants within the plots. Each census year is a sample of interannual climatic variation ($n = 14$ years). We fit vital rate models as hierarchical Bayesian generalized linear mixed models using RStan (39) to isolate endophyte effects on vital rate means and variances, borrow strength across species for some variance components, and propagate uncertainty from the vital rate estimates to our population model (40). We then parameterized stochastic matrix population models for each of the seven grass host species from the vital rate regressions to comprehensively quantify endophyte effects on growth rates and decompose the overall effect of the symbiosis into contributions through mean vital rates, variance in vital rates, and their interaction (Supplemental Material describes the statistical methods in full).

Across seven host species, eight vital rates, 14 years, and 16,789 individual plants, we found that endophyte symbiosis consistently altered the mean and variance of host vital rates. Endophytes had a positive effect on the mean for 64% (36/56) of host species–vital rate combinations (average Cohen’s D for effects on vital rate mean: 0.15), and benefits were particularly strong for host survival, plant growth and germination (Fig. 1A). Endophytes also reduced inter-annual variance for the majority of host species and vital rates (37 / 56; Fig. 1A), providing the first

empirical support for the hypothesis of symbiont-mediated variance buffering (average Cohen's D for effects on vital rate standard deviation: -0.15). The relative magnitude of symbiont effects on means versus variances differed among grass species and their vital rates. For example, endophytes modestly increased mean adult survival (Fig. 1C) and reduced variance in survival (Fig. 1D) for *Festuca subverticillata*, while for *Poa alsodes*, variance buffering was more apparent in seedling growth and in inflorescence production (Fig 1E). Interestingly, there were also certain vital rates that showed costs of endophyte symbiosis. Symbiotic individuals of *A. perennans* grew larger between censuses than those without endophytes (Fig. 1B), yet endophytes also reduced this species' mean germination rates (Fig. 1A). Similarly, endophyte symbiosis increased variance in seedling growth for *Elymus villosus* and *Festuca subverticillata* (Fig. 1B).

We used stochastic matrix models with plant size (tiller number) as the integer-valued state variable to integrate the diverse effects on vital rates described above into comprehensive measures for the mean and variance of population growth rate (λ) because not all vital rates contribute equally to population growth. On average across host species, endophyte-symbiotic populations had 9% greater mean growth rates, $\bar{\lambda}$, than endophyte-free populations (Fig. 2A). Our hierarchical Bayesian analysis, which propagates uncertainty from the underlying data through model predictions, indicated 92% confidence that endophytes increased $\bar{\lambda}$. The coefficient of variation of λ , reflecting inter-annual variability in population growth rates, was 40% lower in endophyte-symbiotic populations than endophyte-free populations, (with 86% confidence that the endophyte effect was dampening) (Fig. 2B). For some host species, the coefficient of variation was reduced by as much as 170% (*P. alsodes*, *F. subverticillata*), while for others, effects were substantially smaller (6% - *E. villosus*, 16% - *A. perennans*), or even slightly positive (27% increase - *E. virginicus*). When the two mechanisms are considered together, none of the host-symbiont pairings were antagonistic (i.e. with endophytes that both decreased mean

and increased variance) (Fig. 2C) suggesting that differences between hosts' mean and variance effects may reflect alternative life history strategies that maximize fitness. We expected symbiotic plants to be less sensitive to drought, as has been reported for some *Epichloë* symbioses (38). Analysis of a climate-explicit population model indicated that for five out of seven taxa, symbiotic populations were less sensitive to annual or growing season drought (12 or 3 month SPEI) (41)) than symbiont-free populations (Fig. S24-S25; Table S3) (Supplemental Methods). However, we did not find a strong relationship between the magnitude of variance buffering effects and relative drought sensitivities. Identifying the potentially complex relationships between vital rates and the environment remains a key challenge for accurate forecasts of the ecological impacts of stochasticity.

Having documented significant benefits of endophyte symbiosis to fitness via mean benefits and variance buffering, we next evaluated the relative importance of these pathways of host-symbiont mutualism for the stochastic growth rate λ_S . We decomposed the overall effect of the symbiosis on λ_S into contributions from mean growth rates or variance buffering effects by estimating λ_S for population models incorporating both mean and variance buffering effects, for mean effects alone, for variance effects alone, and for models with no endophyte effects. We ran each simulation for 1000 years by randomly sampling from the annual transition matrices observed over the 14 year experiment, discarding the first 100 years to remove transient dynamics. Sampling observed transition matrices leads to models which realistically capture interannual variation by preserving correlations between individual vital rates (42). We calculated λ_S for each host species as the mean of annual growth rates during each simulation. This decomposition provided strong evidence of mutualism for endophyte symbiosis when averaging each contribution across species (100% certainty of a positive total effect on λ_S) (Fig. 3). Contributions to the full effect of symbiosis on λ_S derived from both mean and variance buffering effects, as well as interactive effects from mean and variance benefits. Effects on the

mean were four times greater on average than contributions from variance buffering. Yet, for two species (*A. perennans*, *P. sylvestris*) contributions from variance buffering exceeded mean effects (Fig. S21).

We next used simulations to project how contributions from mean fitness effects and variance buffering change under scenarios of increased variability, a key prediction of climate change. Under the regime of environmental variability observed over the course of this study, endophyte effects on mean population growth rates were the primary contribution to mutualistic outcomes. To simulate increased variability, we repeated the estimation of λ_S under two scenarios, choosing the transition matrices of the six or two most extreme years experienced by symbiont-free plants, compared to the ambient scenario that included all 14 observed years. These treatments increased the standard deviation of yearly growth rates during simulations by 1.3, or 2.1 times relative to the ambient scenario, while maintaining equivalent mean growth rates (< 2.3% difference between simulation treatments)(See SM; Fig. S22). Under increased variability, endophyte symbiosis provided stronger mutualistic benefits (Fig. 3) than under ambient variability, driven by increasing contributions from the variance buffering mechanism (from a 24% contribution in ambient scenario to a 66% contribution in the most extreme scenario), while the overall effect of the symbiosis increased by > 130% under increased variance. This result suggests that mutualism with *Epichloë* endophytes in general, and their variance buffering effect in particular, will take on increased importance for grasses in a more variable climate future.

Life history variation is a potential explanation for differences in strategy across plant-endophyte symbiota. Long-lived species, those on the slow end of the slow-fast life history continuum, are expected to be less sensitive to environmental variability (43), a pattern which has empirical support across plants (44) and animals (45). Therefore, we predicted that host species with slower life histories (producing fewer, larger offspring that persist through en-

vironmental variability) would benefit less from the variance buffering effects of endophytes than species with fast life histories (producing many offspring with low per-capita chance of success) (46, 47). We calculated demographic life history traits (generation time, longevity, and net reproductive rate) from matrix models for symbiont-free populations using the Rage package (48) and we collated other traits from the literature (seed length) and from the experimental plots (99th percentile of maximum observed age). We used Bayesian phylogenetic mixed-effects models to assess the relationship between these traits and the variance buffering effect of symbiosis, propagating uncertainty associated with estimated variance buffering effects (Supplemental Methods). In general, symbiota with trait values representing faster life history strategies experienced greater variance buffering from endophytes (Fig. 4) than those with fast life histories, as predicted. For example, variance buffering was stronger for host species with smaller seeds (Fig. 4E; 74% probability of positive relationship) and shorter longevity (Fig. 4C; 64% probability of positive relationship). Other life history traits showed similar small but positive support for the prediction that slower life traits would correlate with stronger variance buffering (Fig. S27). Additionally, in our study, the three host species for which the overall mutualism was weakest (*Elymus villosus*, *Elymus virginicus*, and *Poa sylvestris*) (Fig. 2C) were the only hosts for which we observed stromata, fungal fruiting bodies capable of horizontal (contagious) endophyte transmission (Table S2), in line with theoretical expectations for strict vertical transmission to drive the evolution of symbiotic mutualisms (22, 49). Conclusions about life histories are limited by traits spanning a relatively narrow range of values due to the small number of species and their shared evolutionary histories. Our understanding of the role of symbiosis in life history theory would be improved by testing for variance buffering effects across a wide span of taxonomic groups (50).

Our analysis of a 14 year experiment on the presence/absence of fungal symbionts demonstrated that heritable microbes can commonly benefit hosts not only through improved mean

fitness, but also as a buffer against environmental variance. Our novel approach integrated individual-level measurements into demographic models within a framework of Bayesian mixed models to newly account for context-dependent biotic interactions that vary through time. Our results deeply inform understanding of organisms' strategies to cope with environmental stochasticity because we identified a role for microbial symbiosis in demographic variance buffering, for the first time. This variance buffering mechanisms may be similarly relevant to the diverse host-microbe symbioses across the tree of life. This work took a novel and important step to improve forecasts on the responses of populations (and symbiota) to increasingly variable environments under global environmental change, and discovered that mutualist-mediated variance buffering is likely to become an increasingly significant component of benefits of symbiosis in future environments.

References

1. IPCC, *Managing the risks of extreme events and disasters to advance climate change adaptation: special report of the intergovernmental panel on climate change. Special Report*. (Cambridge University Press, 2012).
2. S. Seneviratne, *et al.* (2012).
3. T. F. Stocker, *et al.*, *Climate change 2013: the physical science basis. Contribution of Working Group I to the Fifth Assessment Report of the Intergovernmental Panel on Climate Change* (Cambridge University Press, 2013), pp. 33–115.
4. R. C. Lewontin, D. Cohen, *Proceedings of the National Academy of Sciences* **62**, 1056 (1969). Publisher: National Academy of Sciences Section: Biological Sciences: Zoology.
5. S. D. Tuljapurkar, *Theoretical Population Biology* **21**, 141 (1982).

6. J. E. Cohen, *Theoretical population biology* **16**, 159 (1979).
7. S. Tuljapurkar, *Population dynamics in variable environments*, vol. 85 (Springer Science & Business Media, 2013).
8. C. A. Pfister, *Proceedings of the National Academy of Sciences* **95**, 213 (1998).
9. W. F. Morris, *et al.*, *Ecology* **89**, 19 (2008).
10. A. Compagnoni, *et al.*, *Ecological Monographs* **86**, 480 (2016).
11. M. M. Ellis, E. E. Crone, *Ecology* **94**, 1681 (2013).
12. R. C. Rodríguez-Caro, *et al.*, *Oikos* **130**, 1346 (2021).
13. S. Tuljapurkar, S. H. Orzack, *Theoretical Population Biology* **18**, 314 (1980).
14. J. Fieberg, S. P. Ellner, *Ecology letters* **4**, 244 (2001).
15. E. S. Menges, *Ecological Bulletins* pp. 73–84 (2000).
16. A. Kuparinen, A. Boit, F. S. Valdovinos, H. Lassaux, N. D. Martinez, *Scientific reports* **6**, 22245 (2016).
17. C. H. Hilde, *et al.*, *Trends in Ecology & Evolution* **0** (2020). Publisher: Elsevier.
18. R. Rodriguez, J. White Jr, A. E. Arnold, a. R. a. Redman, *New phytologist* **182**, 314 (2009).
19. M. McFall-Ngai, *et al.*, *Proceedings of the National Academy of Sciences* **110**, 3229 (2013).
20. L. J. Funkhouser, S. R. Bordenstein, *PLoS biology* **11**, e1001631 (2013).
21. P. W. Ewald, *Annals of the New York Academy of Sciences* **503**, 295 (1987).
22. P. E. Fine, *Annals of the New York Academy of Sciences* **266**, 173 (1975).

23. J. A. Russell, N. A. Moran, *Proceedings of the Royal Society B: Biological Sciences* **273**, 603 (2006).
24. J. C. Brownlie, K. N. Johnson, *Trends in microbiology* **17**, 348 (2009).
25. S. N. Kivlin, S. M. Emery, J. A. Rudgers, *American Journal of Botany* **100**, 1445 (2013).
26. C. Corbin, E. R. Heyworth, J. Ferrari, G. D. Hurst, *Heredity* **118**, 10 (2017).
27. K. D. Hoadley, *et al.*, *Scientific Reports* **9**, 1 (2019).
28. S. A. Chamberlain, J. L. Bronstein, J. A. Rudgers, *Ecology letters* **17**, 881 (2014).
29. P. Jordano, *Oikos* pp. 479–491 (1994).
30. I. Billick, K. Tonkel, *Ecology* **84**, 289 (2003).
31. J. A. Rudgers, *et al.*, *Annual review of ecology, evolution, and systematics* **51** (2020).
32. A. Leuchtmann, *Natural toxins* **1**, 150 (1992).
33. G. P. Cheplick, S. Faeth, S. H. Faeth, *Ecology and evolution of the grass-endophyte symbiosis* (OUP USA, 2009).
34. J. A. Rudgers, *et al.*, *Ecology* **90**, 1531 (2009).
35. D. Brem, A. Leuchtmann, *Oecologia* **126**, 522 (2001).
36. G. P. Cheplick, *American Journal of Botany* **91**, 1960 (2004).
37. S. Kannadan, J. Rudgers, *Functional Ecology* **22**, 706 (2008).
38. F. A. Decunta, L. I. Pérez, D. P. Malinowski, M. A. Molina-Montenegro, P. E. Gundel, *Frontiers in plant science* **12**, 644731 (2021).

39. Stan Development Team, RStan: the R interface to Stan (2022). R package version 2.21.7.
40. B. D. Elderd, T. E. Miller, *Ecological Monographs* **86**, 125 (2016).
41. S. M. Vicente-Serrano, S. Beguería, J. I. López-Moreno, *Journal of climate* **23**, 1696 (2010).
42. C. J. E. Metcalf, *et al.*, *Methods in Ecology and Evolution* **6**, 1007 (2015).
43. G. I. Murphy, *The American Naturalist* **102**, 391 (1968).
44. A. Compagnoni, *et al.*, *Nature communications* **12**, 1 (2021).
45. C. Le Coeur, N. G. Yoccoz, R. Salguero-Gómez, Y. Vindenes, *Ecology Letters* **25**, 2107 (2022).
46. M. Rees, *Philosophical Transactions of the Royal Society of London. Series B: Biological Sciences* **351**, 1299 (1996).
47. A. T. Moles, M. Westoby, *Journal of Ecology* **92**, 372 (2004).
48. O. R. Jones, *et al.*, *Methods in Ecology and Evolution* **13**, 770 (2022).
49. M. E. Afkhami, J. A. Rudgers, *The American Naturalist* **172**, 405 (2008).
50. J. M. Jeschke, H. Kokko, *Evolutionary Ecology* **23**, 867 (2009).
51. C. W. Bacon, J. F. White, *Biotechnology of endophytic fungi of grasses* (CRC Press, 2018), pp. 47–56.
52. J. A. Rudgers, A. L. Swafford, *Basic and Applied Ecology* **10**, 43 (2009).
53. S. P. Brooks, A. Gelman, *Journal of computational and graphical statistics* **7**, 434 (1998).

54. A. Gelman, J. Hill, *Data analysis using regression and multilevel/hierarchical models* (Cambridge university press, 2006).
55. J. L. Williams, T. E. Miller, S. P. Ellner, *Ecology* **93**, 2008 (2012).
56. H. Caswell, *Inc., Sunderland, MA* (2001).
57. M. Rees, S. P. Ellner, *Ecological Monographs* **79**, 575 (2009).
58. S. Chamberlain, D. Hocking, B. Anderson (2022).
- 59.
60. P.-C. Bürkner, *Journal of Statistical Software* **80**, 1 (2017).
61. A. E. Zanne, *et al.*, *Nature* **506**, 89 (2014).
62. A. Leuchtmann, C. W. Bacon, C. L. Schardl, J. F. White Jr, M. Tadych, *Mycologia* **106**, 202 (2014).

Acknowledgments

We thank the many individuals who contributed to field data collection.

Supplementary materials

Materials and Methods

Figs. S1 to S10

Tables S1 to S3

References (51-62)

Material and Methods

Study site and species This study was conducted at Indiana University's Lilly Dickie Woods (39.238533, -86.218150) in Brown County, Indiana, USA. This site is part of the Eastern broadleaf forests of southern Indiana where the ranges of many cool-season grass species overlap. The experiment focused on seven of these grasses which host *Epichloë* endophytes (*Agrostis perennans*, *Elymus villosus*, *Elymus virginicus*, *Festuca subverticillata*, *Lolium arundinaceum*, *Poa alsodes*, and *Poa sylvestris*) (Table S1).

Endophyte removal, plant propagation, and planting methods Seeds from naturally symbiotic populations of the seven focal host species were collected during the 2006 growing season from Lilly Dickie Woods (39.238533, -86.218150) and the Bayles Road Teaching and Research Preserve (39.220167, -86.542683) in Brown County, Indiana, USA. To generate symbiotic (S+) and symbiont-free (S-) plants that shared the same genetic lineage, the collected seeds from each species were sterilized with a heat treatment (as described in Table S1) or left untreated. The heat treatment is intended to create symbiont-free plants by bringing seeds to temperature at which the fungus becomes inviable but the host seeds can successfully germinate. Both heat-treated and untreated seeds were surface sterilized with bleach and cold stratified for up to 4 weeks, then germinated in a growth chamber before being transferred to the greenhouse at Indiana University and allowed to grow for 8 weeks. We confirmed the endophyte status of these plants using microscopy of leaf peels, where tissue from the leaf sheath is stained with aniline blue dye and examined for the presence of fungal hyphae at 100X magnification (51). Then, we established the experimental plots with vegetatively propagated clones of similar sizes from the plants². By starting the experiment with plants of similar sizes, we aimed to limit potential negative side effects of heat treatments on the growth of plants in our experiment (52).

²not sure this happened

During the fall of 2007 and spring of 2008, we established 10 3x3 m. plots for *A. perennans*, *E. villosus*, *E. virginicus*, *F. subverticillata*, and *L. arundinaceum* and 18 plots for *P. alsodes* and *P. sylvestris*. For each species, five (or nine, for *P. alsodes* and *P. sylvestris*) plots were randomly assigned to be planted with either symbiotic (S+) or with symbiont-free (S-) plants. Each plot was planted with 20 evenly spaced S+ or S- individuals and each plant received a unique aluminum tag staked into the ground. In XXXX, we placed fencing around each plot to limit herbivory and disturbance in the plots, and replaced fencing for all plots in XXXX.³

Long-term demographic data collection Each summer starting in 2008 through 2021, we censused all individuals in each plot for survival, growth and reproduction. We censused each species during its flowering period (May: *Poa alsodes*, *Poa sylvestris*; June: *Festuca subverticillata*; July: *Elymus villosus*, *Elymus virginicus*, *Lolium arundinaceum*; September: *Agrostis perennans*), such that the censuses were pre-breeding and marked new recruits from the previous years' recruitment . Leaf litter was cleared out of each plot prior to the census, to aid in locating all tagged individuals and new recruits. For each plant remaining from the previous year, we marked its survival, measured its size as a count of the number of tillers, and collected reproductive data by counting the number of reproductive tillers, and then counting the number of seed-bearing spikelets on up to three of those reproductive tillers. In each plot, we also searched for and tagged any unmarked individuals, which are recruits from the previous years' seed production, for which we collected the same demographic data. New recruits typically have one tiller and are non-reproductive. In 2008 and 2009, we took additional counts of seeds per inflorescence for all reproducing individuals in the plots. For *Agrostis perennans*, we also collected seed counts in 2010. In 2018, we ceased data collection for *Lolium arundinaceum* which had very high survival in the experimental plots and consequently very low

³

variation across years. For each individual plant in the experiment, we have data recording their transitions in size and reproduction from one year to the next. In total across 14 years, the dataset includes demographic information for 16789 individual host-plants making up 31,216 individual transition years.

We typically expect plots to maintain their endophyte status (S+ or S-) because the fungal symbionts are almost entirely vertically transmitted and plots are **spaced at least 5 m apart**, limiting the possibility of dispersal between plots or horizontal transmission of the symbiont. Seeds from reproductive individuals were taken opportunistically from reproducing plants throughout the experiment. These seeds were scored with microscopy for their endophyte status (100X magnification with analine blue dye). Overall, these scores reflect a 97.5% faithfulness of recruits to their expected endophyte status across species and plots (Fig. S23; Supplement data). Additionally, over the course of the experiment, we have rarely observed fungal stromata, the fruiting bodies by which *Epichloë* are potentially transmitted horizontally. For *A. perennans*, *F. subverticillata*, *L. arundinaceum*, and *P. alsodes*, we have never observed stromata. We have observed stromata only infrequently for *E. villosus*, and even more rarely for *E. virginicus* and *P. sylvestris* (Table S2). For these species, stromata have only been observed on 35, 4, and 6 plants respectively, making up less than 0.3% of all censused plants (Supplemental data). These stromata observations occurred irregularly across years; in most years there were no stromata, and in a few years several plants produced stromata during the census.

Vital rate modeling Equiped with this demographic data, we next fit statistical models for survival, growth, flowering (yes or no), fertility of flowering plants (no. of flowering tillers), production of seed-bearing spikelets (no. per inflorescence), the average number of seeds per spikelet, and the recruitment of seedlings from the preceeding year's seed production (Fig. S1 - S10). We fit these vital rates as generalized linear mixed models, including a random year

effect, with separate estimates of variance for symbiotic and symbiont-free plants, to quantify the effect of endophytes on interannual variance (Fig. S11 - S18). These random effects and other predictors as described below were given vague priors. We ran each vital rate model for 2500 warm-up and 2500 MCMC sampling iterations with three chains using RStan (39). We assessed model convergence with trace plots of posterior chains and checked for \hat{R} values less than 1.01, indicating low within- and between-chain variation (53, 54). For those models that showed poor convergence, we extended the MCMC sampling to include 5000 warm-up and 5000 sampling iterations, which was only necessary for seedling growth. For each of these vital rate models, we graphically checked model fit with posterior predictive checks comparing simulated data from 500 posterior draws with the observed data (Fig. S19-S20)

Survival - We modeled survival as a Bernoulli process, where the survival (S) of an individual i in census year t was predicted by the plot-level endophyte status (e), its host species (h), its size in the preceding census (x), and the plants origin status (whether it was initially transplanted or was naturally recruited into the plot) .

$$S_{i,p,(e),h,t} \sim Bernoulli(\hat{S}_{p,(e),h,t}) \quad (2a)$$

$$\text{logit}(\hat{S}_{p,(e),h,t}) = \beta_{0(e),h} + \beta_1 * \text{origin}_i + \beta_2 * x_i + \beta_3 * x_i * \text{species}_h + \tau_{(e),h,t} + \rho_p \quad (2b)$$

$$\tau_{(e),h,t} \sim Normal(0, \sigma_{\tau_{(e),h}}^2) \quad (2c)$$

$$\rho_p \sim Normal(0, \sigma_\rho^2) \quad (2d)$$

Here, \hat{S} is the survival probability, $\beta_{0(e),h}$ is an intercept specific to each host species and endophyte status, β_1 is the effect of the plant's recruitment origin, β_2 and β_3 define the size-dependent slope for each species, $\tau_{(e),h,t}$ is a normally distributed year effect for each species and endophyte status with variance $\sigma_{\tau_{(e),h}}^2$ for each species and endophyte status, and ρ_p is a normally distributed plot effect for each plot p with variance σ_ρ^2 shared across species. We

separately modeled the survival of newly recruited seedlings, which were typically one tiller and non-reproductive, with a similar model omitting size structure and the effect of the plant's origin status.

Growth - We modeled plant size in census year t (G) with the same predictors as described for survival. Because we measured size as positive integer-valued counts of tillers, we modeled it with a zero-truncated Poisson-inverse Gaussian distribution. This distribution includes an additional shape parameter λ_G to account for overdispersion in the data. We additionally modeled the growth of newly recruited seedlings separately with a model omitting size structure and the plants' origin status as with seedling survival.

Flowering - We modeled whether or not a plant was flowering during the census (P) as a Bernoulli process, in a similar manner as described above except that size structure for reproductive vital rates was determined by the individual's size during the census as opposed to the size during the preceding census.

Fertility - For a plant that was flowering during the census, its fertility was the number of reproductive tillers produced (F), which we modeled with a Poisson-Inverse Gaussian distribution, parameterized as described above.

Spikelets per Inflorescence - We fit data on spikelet production (K) which is recorded as integer counts on up to three inflorescences per reproducing plant with a negative binomial distribution, parameterized as described above.

Seed Production - For individuals with recorded counts of seed production, we calculated the number of seeds per spikelet from our counts of seeds and spikelets per inflorescence, and then modeled seeds per spikelet (D) as normally distributed averages for each species and endophyte status. Because we had less detailed data across years and plants for seed production than for other reproductive vital rates, we omitted both plot and year random effects.

Seedling Recruitment - Finally, we used a binomial distribution to model the recruitment of

new seedlings (R) into the plots from seeds produced in the preceding year. We included an intercept specific to each host and endophyte status and the same random effects structure as in other models. We estimated the number of seeds per plot in the preceding year by multiplying the number of reproductive tillers for each plant by the mean number of spikelets per inflorescence and by a sample from the posterior distribution of mean number of seeds per spikelet (D). For plants with missing fertility or spikelet data, we used the expected number of reproductive tillers (F) or of spikelets per inflorescence (K), drawing from the full posteriors of our models. We rounded this value to get the estimated seed production for each individual, and finally summed across all reproductive plants in each year and plot to get the total number of seeds produced.

Stochastic population model Using the fitted vital rate models, we parameterized stochastic matrix population models for each species including two state variables: $r_{h,t}$ (the number of newly recruit individuals in year t), and $\mathbf{n}_{h,t}$ (a vector including all non-seedling individuals of sizes $x \in \{1, 2, \dots, U_h\}$, ranging from one tiller up to the maximum size U_h . The total number of recruits in year $t + 1$ is given by:

$$r_{h,t+1} = \sum_{x=0}^{U_h} P(x; \boldsymbol{\tau}_P) F(x; \boldsymbol{\tau}_F) K(x; \boldsymbol{\tau}_K) D R(\boldsymbol{\tau}_R) n_{x_{h,t}} \quad (3)$$

The total number of seeds produced by a maternal plant of size x is the product of the size-specific probability of flowering P , the number of reproductive tillers F , the number of spikelets per inflorescence K , and the number of seeds per spikelet D . Multiplying by the probability of transitioning from seed to seedling R gives a per-capita rate of seedling production for each species h , which is multiplied by the number of plants of size x ($n_{x_{h,t}}$, the x^{th} element of $\mathbf{n}_{h,t}$) and summed. Each function also depends on the intercept parameter specific to each endophyte status and species, as well as the endophyte-specific year random effects ($\boldsymbol{\tau}$) for that vital rate.

Survival and growth determine the rest of the population dynamics of the new seedlings and larger plants. The number of y -sized plants is given by:

$$n_{h,t+1}^y = Z(y)B(y; \boldsymbol{\tau}_B)R_t + \sum_{x=0}^{U_h} S(x; \boldsymbol{\tau}_S)G(x, y; \boldsymbol{\tau}_G) \quad (4)$$

where $n_{h,t+1}^y$ is the y^{th} element of vector \mathbf{n} for species h . The survival (Z) and growth (B) of seedling recruits, where $Z(y)$ is the size distribution of recruits that survive their first year is the first term on the right hand side of Eqn. 4. This is added to the survival of x -sized plants and the growth of survivors from size x to y , summed over all x . To avoid predictions of unrealistic growth outside of the observed size distribution, we set a ceiling on the growth function for plants above the 97.5th percentile in the observed size distribution (55). Each of the functions in Eqns. 3 and 4 have separate intercepts and year random effects for symbiotic and symbiont-free populations, allowing us to calculate the effect of endophyte symbiosis on the mean and variance of population growth rates, λ , the dominant eigenvalue of the projection matrix.

Mean-variance decomposition and simulation experiment To calculate stochastic population growth rates for each host species, λ_s , we simulated population dynamics for 1000 years by randomly sampling from the annual transition matrices observed over the course of the experiment, discarding the first 100 years to remove transient dynamics. We tallied the total population size at each time step as $N_{[h,t]} = r_{[h,t]} + \sum_o^{U_h} n_{x[h,t]}$ and calculated the stochastic growth rate as $\log(\lambda_s) = E[\log(\frac{N_t}{N_{t+1}})]$ (56, 57). To calculate the total effect of endophyte symbiosis and attribute this effect to the mean and variance buffering mechanisms, we ran this simulation for populations with endophyte effects on the mean and variance, on the mean alone, on the variance alone, and for symbiont-free populations without either endophyte effect. We repeated these simulations and propagated uncertainty from the vital rate models for 500 draws from the posterior of model parameters. The contributions are then the difference in long-term growth rates between models with the mean and variance. There is also an interaction between mean

and variance effects, which makes sense in light of Eqn. 1. The variance penalty to stochastic growth is proportional to the mean value of annual growth rates such that variance is more detrimental for populations with low average growth rates.

To create scenarios of increased variance relative to that observed during the study period, we repeated the stochastic growth rate decomposition sampling only a subset of observed annual transition matrices. We created two scenarios by altering the sampled transition matrices . We sampled the six, or two transition matrices associated with the lowest and highest growth rates for symbiont-free populations. As the number of years sampled for the simulations decreased, the mean value of growth rates remained similar (less than 2.3% difference in the mean of annual growth rates) (Fig. S22A), while the standard deviation more than doubled on average across species (Fig. S22B). We performed the same decomposition for these scenarios as for the ambient conditions for all host species, and then calculated the mean across species for the different contribution elements.

Estimating climate drivers of environmental context-dependence To connect the variance buffering effects of endophytes with interannual climatic variability, we built climate-explicit stochastic matrix population models from the vital rate data. To do this, we first downloaded temperature and precipitation data from the weather station in Bloomington, IN, approx. 27 km from our study site, using the rnoaa package (58). Compared to other weather stations in the area, the measurements from Bloomington contain the most complete climate record across the study period, and are correlated with more local measurements from Nashville, IN (total annual precipitation: $R^2 = .60$; mean annual temperature: $R^2 = .62$). The mean annual temperature across the study period was is $11.9 C^\circ$ (SD: $1.05 C^\circ$) and the average annual precipitation was 1237.9 mm/year (SD: 204.89 mm/year) Given endophytes known role in drought tolerance, we calculated the Standardised Precipitation-Evapotranspiration Index for 3 and 12 months

preceding each annual censuses, reflecting drought during the growing season and across the year (41).

We repeated the process of fitting statistical models for each vital rate as described above with the inclusion of a slope parameter describing the relationship with the climate driver. We fit separate vital rate models incorporating either the growing season or annual drought index for each vital rate, except for the model describing the mean number of seeds per inflorescence. This model was fit without climate effects because the data came from only a few years. Initial analyses indicated similar model fits for models including only a linear term and those with both linear and quadratic terms describing the relationship between the climate driver and the vital rate response, and so we proceeded with models including only the linear term. We expected that including annual climate predictors into the models would explain some interannual variance in vital rates, shrinking the variance associated with the fitted year random effects. We assessed model fit with graphic posterior predictive checks and convergence diagnostics as described for the climate-implicit analysis. Finally, we next built matrix projection models incorporating the climate-dependence to assess the response of symbiotic vs symbiont-free populations to drought. The model is as described above with the inclusion of parameters describing the slope of the relationship with SPEI.

These drought indices did not explain the full extent of interannual variability experienced by the focal populations. However, we compared the sensitivity to either annual or season SPEI of symbiotic growth rates ($\frac{\Delta\lambda_{S+}}{\Delta SPEI}$) with those of symbiont-free populations ($\frac{\Delta\lambda_{S-}}{\Delta SPEI}$)(Fig. S25; Table S3). Most species were slightly more responsive to growing season rather than annual drought conditions, and had sensitivities suggesting that symbiotic populations are less sensitive to drought conditions. *Festuca subverticillata* and *Poa sylvestris* benefited more from symbiosis under wet rather than dry conditions (Fig. S25; Table S3).

Life History Analysis We collected metrics describing each host’s life history to test the relationship between pace of life and variance buffering (Table S3). Using the Rage package, we calculated R_0 , longevity, and generation time from the matrix models for symbiont-free plants. We recorded seed length measurements as the average lemma length from the Flora of North America (59). We also calculated the maximum observed age and the 99th percentile of maximum observed age for each species of symbiont-free plants. Next, we fit Bayesian phylogenetic mixed-effects models using the ‘brms’ package (60) to test the relationship between each life history trait and the estimated effect of symbiosis on the coefficient of variation from the population model while controlling for phylogenetic non-independence in the hosts (Fig. 4) and the symbiont (Fig. S26). We pruned larger species-level phylogenies of plants (61) and *Epichloë* fungi (62) to include the focal species. *Agrostis perennans* was not included in the tree, and so we used a congeneric species. We defined separate phylogenetic covariance matrices for each pruned tree. We propagated uncertainty in the estimated variance buffering effect with a measurement error model and used weakly informative priors to aid model convergence. Each prior was centered at zero, except for the overall standard deviation, which we centered at the standard deviation of the estimated variance buffering effect, .04417872. Thus the model for the variance buffering effect B was given by:

$$B_{estimated,i} \sim Normal(\mu_i, \sigma) \quad (5a)$$

$$\mu = \alpha + \beta * trait + \pi \quad (5b)$$

$$B_{posterior\ mean,i} \sim Normal(B_{estimated,i}, B_{posterior\ sd,i}) \quad (5c)$$

$$\alpha \sim Normal(0, .5) \quad (5d)$$

$$\beta \sim Normal(0, .1) \quad (5e)$$

$$\sigma \sim Half - Normal(.04417872, .01) \quad (5f)$$

$$\pi \sim Normal(0, \sigma_{pi} * \mathbf{A}) \quad (5g)$$

$$\sigma_{pi} \sim Half - Normal(0, .1) \quad (5h)$$

Here, the model includes an intercept parameter (α), and a slope parameter (β) defining the relationship between the variance buffering effect and the life history trait. The overall standard deviation is given by (σ). The phylogenetic random effect (π) has a standard deviation (σ_{pi}) which is structured by the covariance matrix \mathbf{A} . We ran each MCMC sampling chain for 8000 warmup iterations and 2000 sampling iterations. We assessed model convergence as described for the vital rate models.

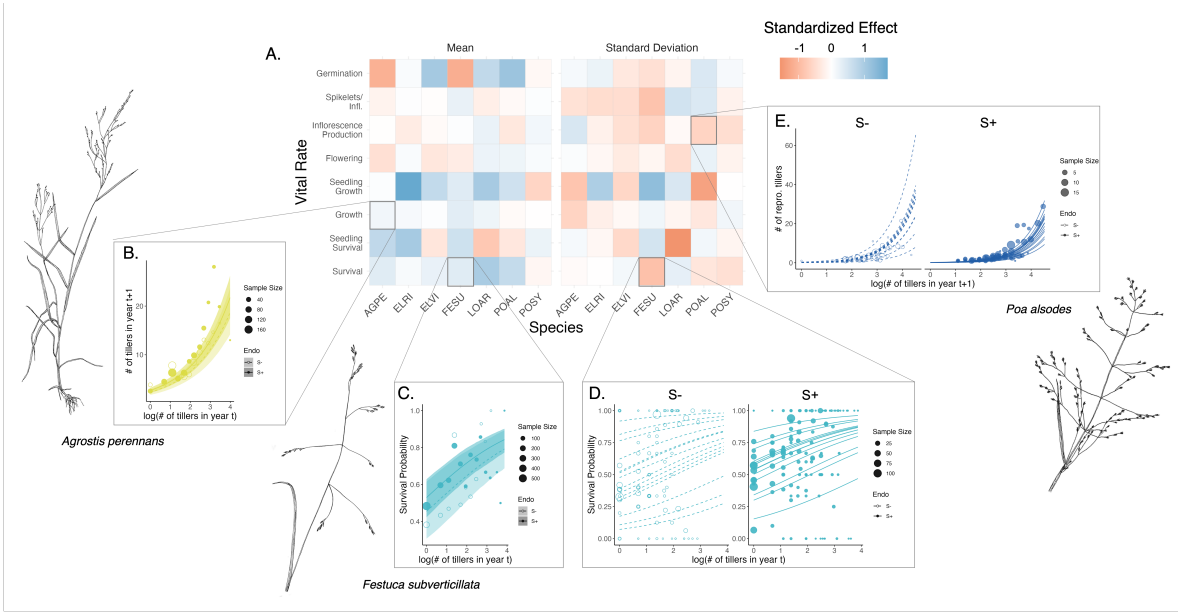


Fig. 1. Endophyte symbiosis altered host vital rates. (A) Shading represents the posterior mean standardized effect size (Cohen's D) of endophyte symbiosis on mean or standard deviation of host vital rates (blue indicates that symbiosis increased the mean or standard deviation and red indicates a reduction). Endophyte presence increased (B) the mean growth rate of *A. perennans* and (C) the survival probability of *F. subverticillata*. Endophyte presence reduced interannual variance in (D) the survival of *F. subverticillata* and (E) the fertility of *P. alsodes*. Organism silhouettes modified from "Festuca subverticillata" by Cindy Roché and "Agrostis hyemalis" and "Poa alsodes" by Sandy Long © Utah State University)

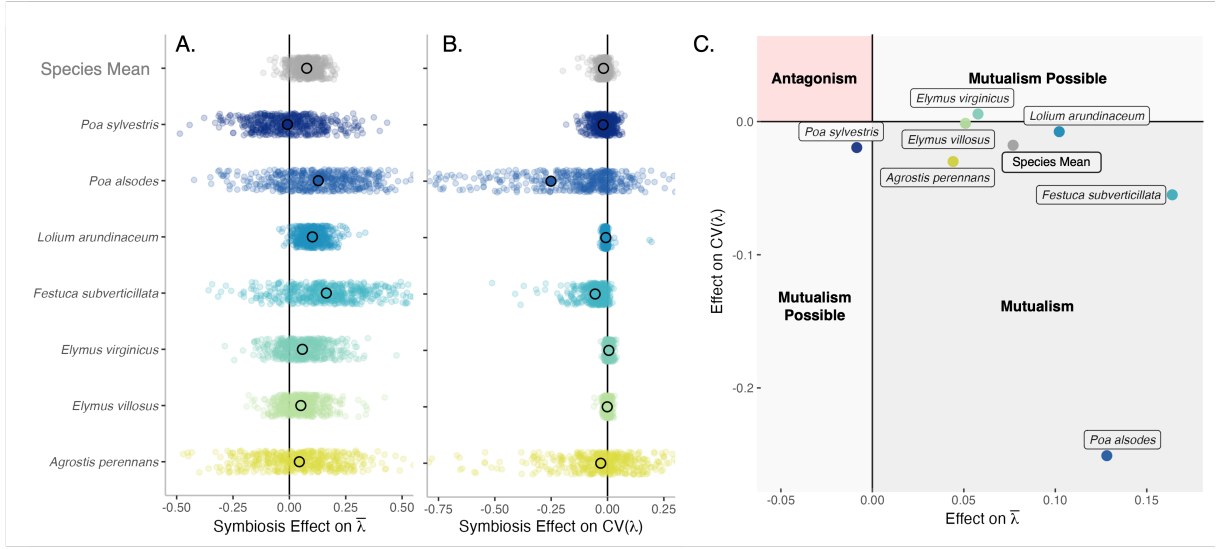


Fig. 2. Mean and variance-buffering effects on population growth rates. Black circles indicate the average effect of endophytes along with 500 posterior draws (smaller colored circles) on the (A) mean and (B) coefficient of variation in population growth rates λ for each host species as well as a cross species mean. (C) For all hosts, endophyte either reduce variance, increase the mean, or both, and consequently when considering stochastic environments, the interactions are always at least potentially mutualistic.

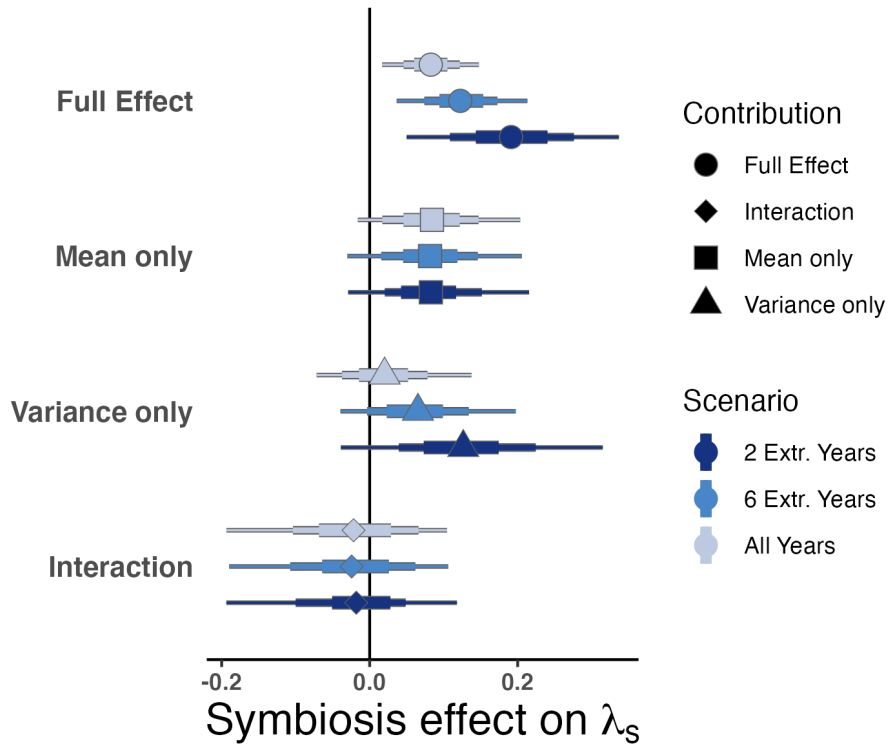


Fig. 3. Endophyte contributions to stochastic growth rates under observed and elevated variance. Endophyte symbiosis contributes to the total effect of mutualism through benefits to mean growth rates and through variance buffering as well as the interaction between mean and variance effects. Shapes indicate the posterior mean of each contribution averaged across the seven focal symbiota, along with bars for the 50, 75 and 95 % credible intervals. The full effect of the symbiosis (circles) becomes more mutualistic under scenarios of increased variance (represented by color intensity). Relative to a scenario sampling transition matrices for all 14 years during the study period, simulations increased variance by sampling the most extreme six or two years, leading to increased contributions from variance buffering effects (triangles) and a constant contribution from mean effects (squares).

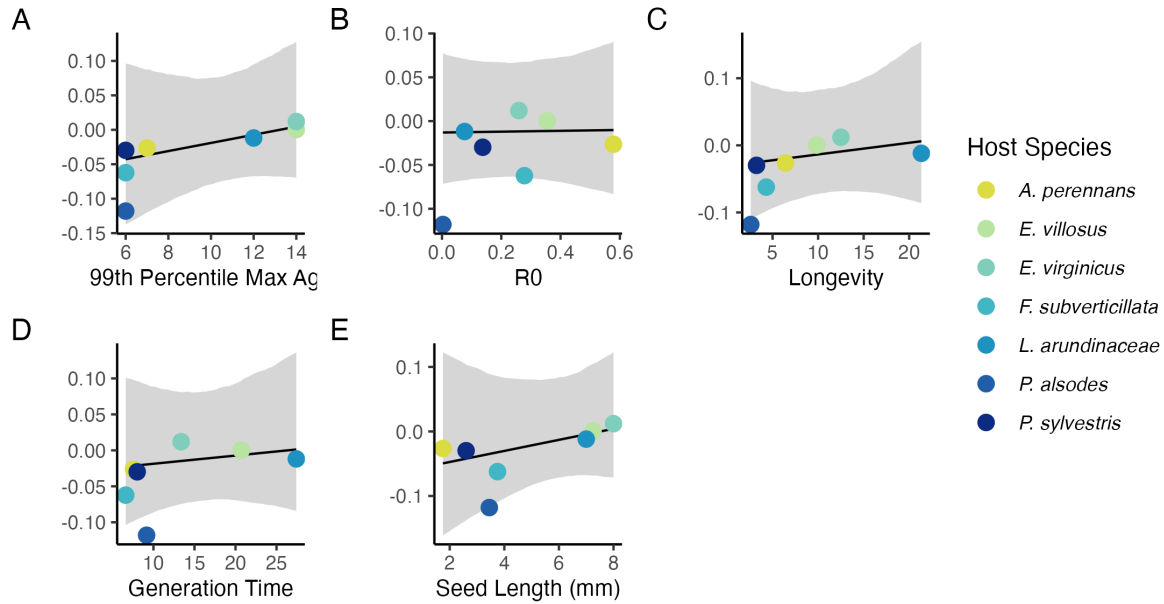


Fig. 4. Host species with faster life history traits experience stronger effects of symbiont-mediated variance buffering. Regressions between life history traits describing the fast-slow life history continuum ((A) Maximum age observed during long term censuses; (B) 99th percentile maximum age during demographic censuses; (C) Net reproductive rate; (D) Longevity; (E) Mean life expectancy; (F) Generation time; (G) Seed size; (H) Rate of imperfect transmission) and the effect of endophyte symbiosis on the coefficient of variation in population growth rate (λ). Each panel shows the fitted mean relationship (line) along with the 95% credible interval.

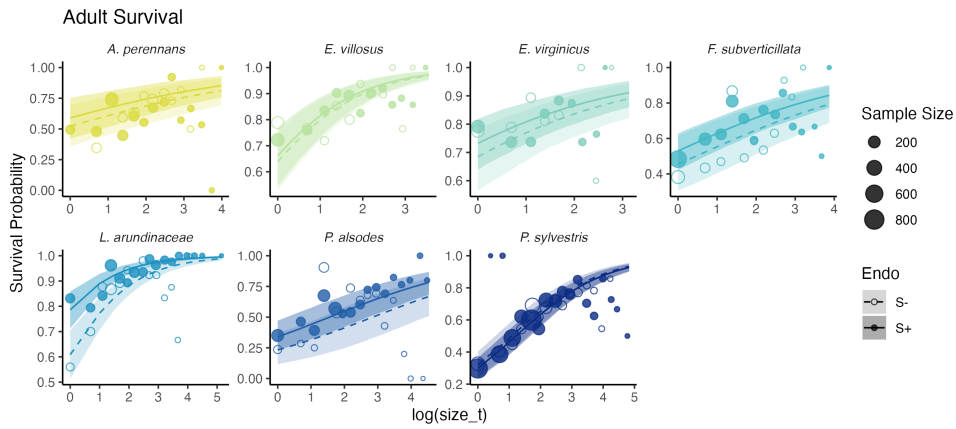


Fig. S1. Effect of endophyte symbiosis on the mean value of adult survival. Fitted curves represent the size-specific mean survival probability along with data binned by size shown as open circles with a dashed line for symbiont-free (S-) plants , while the solid line and filled circles represent symbiotic (S+) plants. 80% credible intervals are shown with dark shading for S+, or light shading for S-.

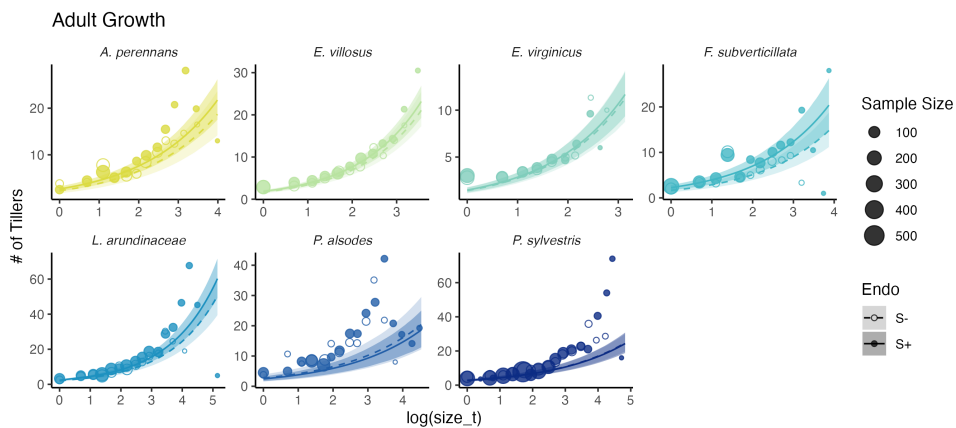


Fig. S2. Effect of endophyte symbiosis on the mean value of adult growth. Fitted curves represent the size-specific mean expected plant size along with data binned by size shown as open circles with a dashed line for symbiont-free (S-) plants , while the solid line and filled circles represent symbiotic (S+) plants. 80% credible intervals are shown with dark shading for S+, or light shading for S-.

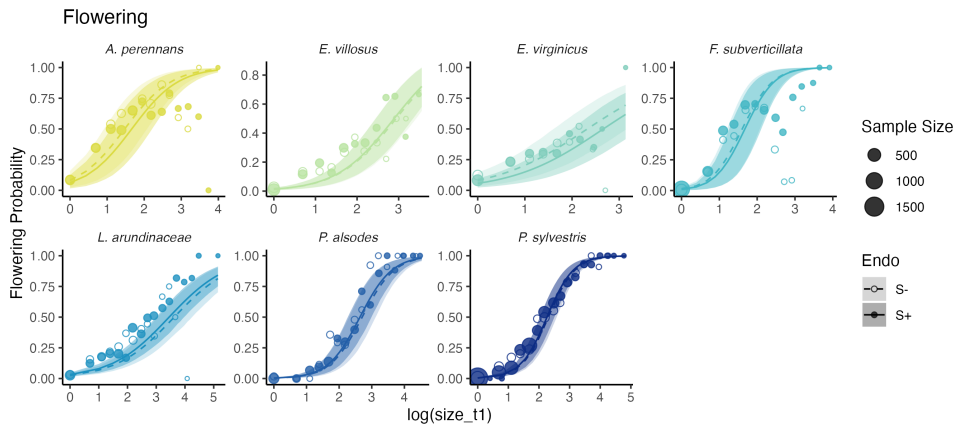


Fig. S3. Effect of endophyte symbiosis on the mean value of flowering Fitted curves represent the size-specific mean flowering probability along with data binned by size shown as open circles with a dashed line for symbiont-free (S-) plants , while the solid line and filled circles represent symbiotic (S+) plants. 80% credible intervals are shown with dark shading for S+, or light shading for S-.

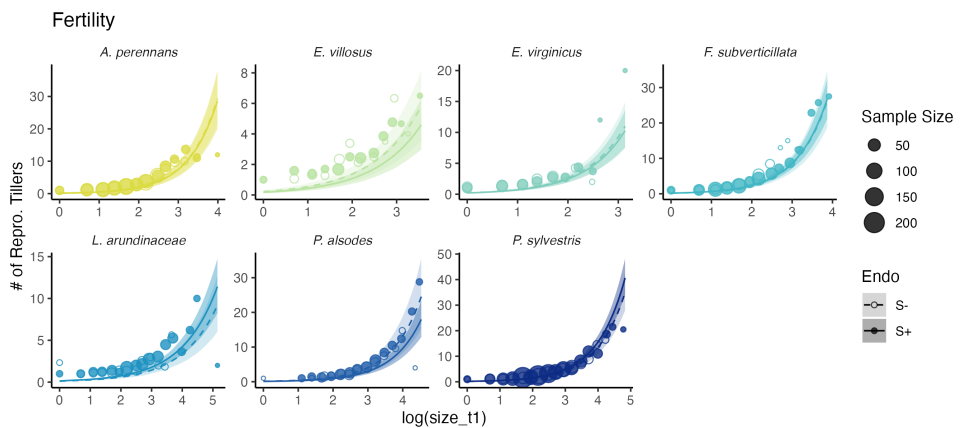


Fig. S4. Effect of endophyte symbiosis on the mean value of fertility. Fitted curves represent the size-specific mean expected number of flowering tillers along with data binned by size shown as open circles with a dashed line for symbiont-free (S-) plants , while the solid line and filled circles represent symbiotic (S+) plants. 80% credible intervals are shown with dark shading for S+, or light shading for S-.

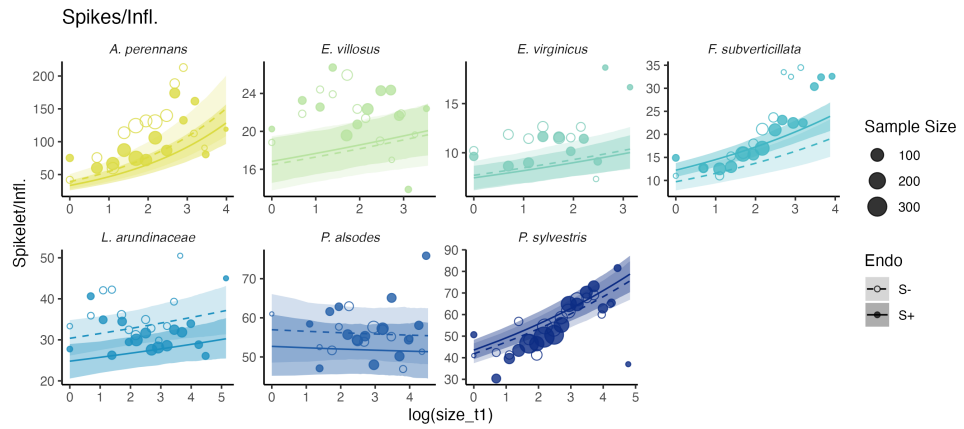


Fig. S5. Effect of endophyte symbiosis on the mean value of spikelet production. Fitted curves represent the size-specific mean expected number of spikelets per inflorescence along with data binned by size shown as open circles with a dashed line for symbiont-free (S-) plants , while the solid line and filled circles represent symbiotic (S+) plants. 80% credible intervals are shown with dark shading for S+, or light shading for S-.

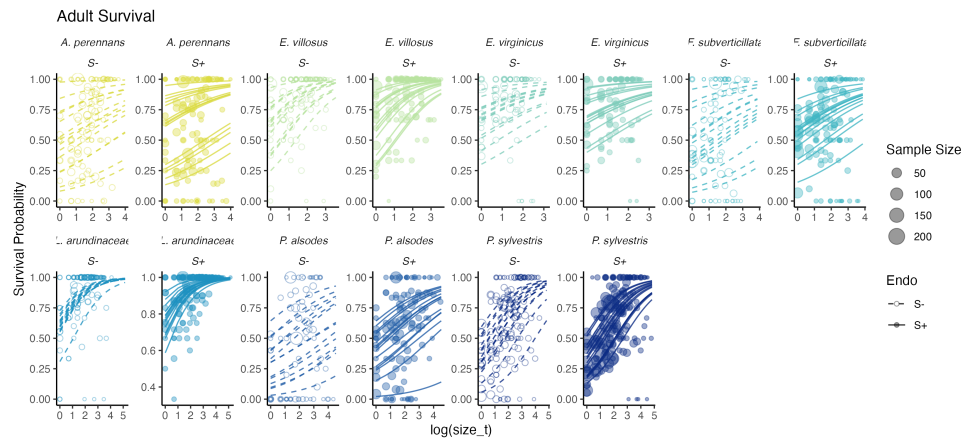


Fig. S6. Effect of endophyte symbiosis on yearly adult survival. Fitted curves represent the size-specific annual survival probability along with data binned by size shown as open circles with a dashed line for symbiont-free (S-) plants , while the solid line and filled circles represent symbiotic (S+) plants.

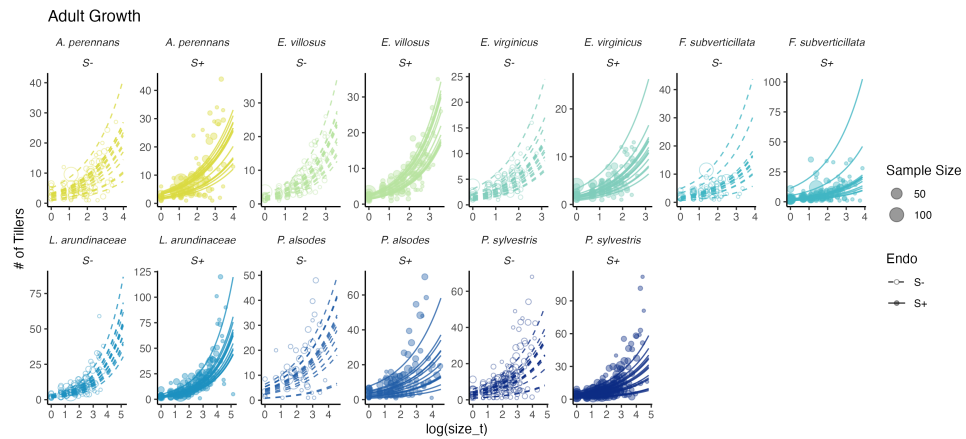


Fig. S7. Effect of endophyte symbiosis on yearly adult growth. Fitted curves represent the size-specific annual expected plant size along with data binned by size shown as open circles with a dashed line for symbiont-free (S-) plants , while the solid line and filled circles represent symbiotic (S+) plants.

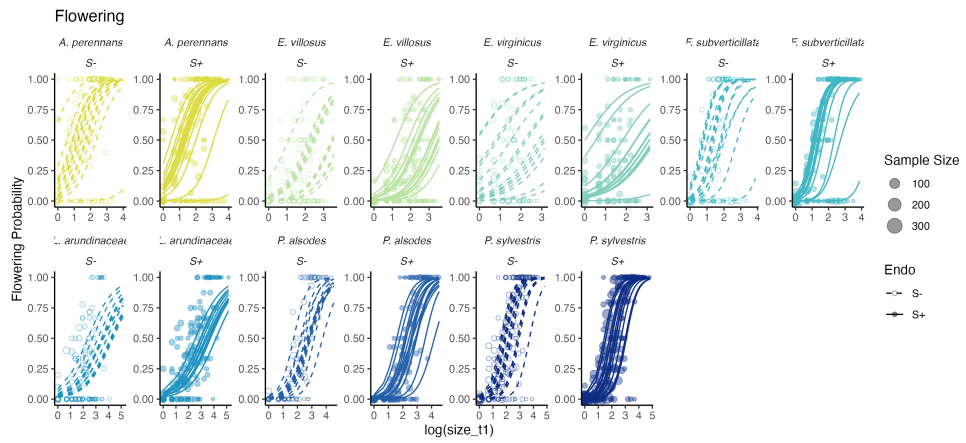


Fig. S8. Effect of endophyte symbiosis on yearly flowering Fitted curves represent the size-specific annual flowering probability along with data binned by size shown as open circles with a dashed line for symbiont-free (S-) plants , while the solid line and filled circles represent symbiotic (S+) plants.

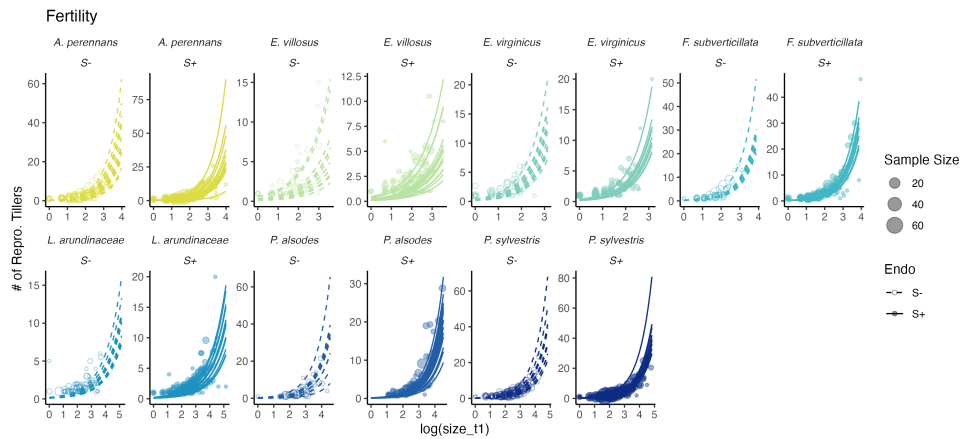


Fig. S9. Effect of endophyte symbiosis on yearly fertility. Fitted curves represent the size-specific annual expected number of flowering tillers along with data binned by size shown as open circles with a dashed line for symbiont-free (S-) plants , while the solid line and filled circles represent symbiotic (S+) plants.

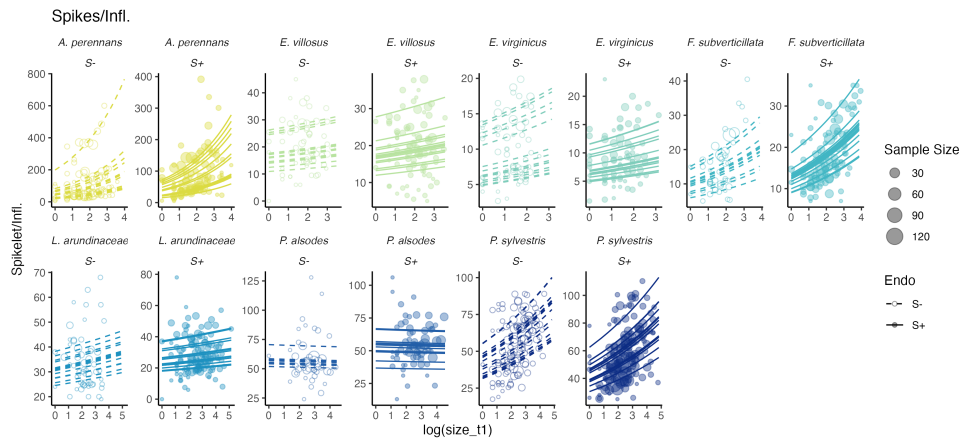


Fig. S10. Effect of endophyte symbiosis on yearly spikelet production. Fitted curves represent the size-specific annual expected number of spikelets per inflorescence along with data binned by size shown as open circles with a dashed line for symbiont-free (S-) plants , while the solid line and filled circles represent symbiotic (S+) plants.

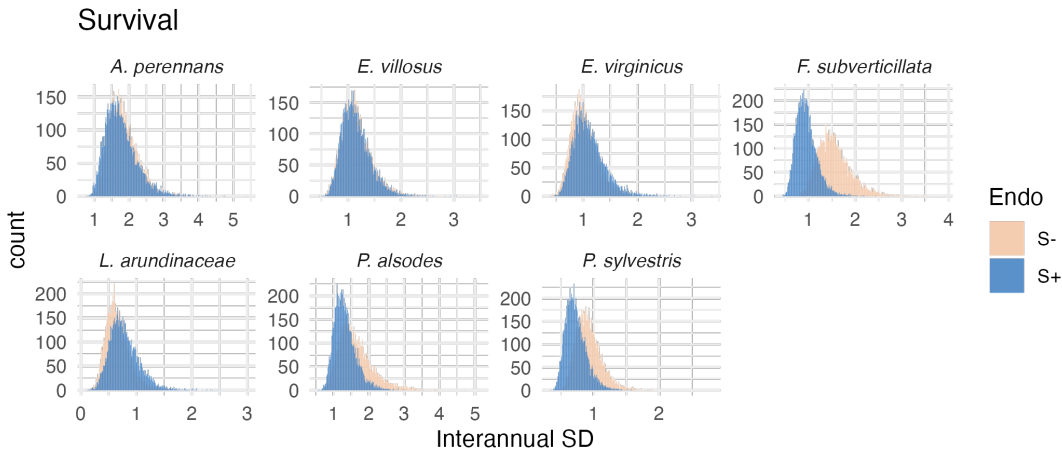


Fig. S11. Posterior distributions of the standard deviations of interannual year effects for survival. Histograms include 7500 post-warmup MCMC samples for symbiotic (S+; blue) and symbiont-free (S-; tan) plants from fitted vital rate model.

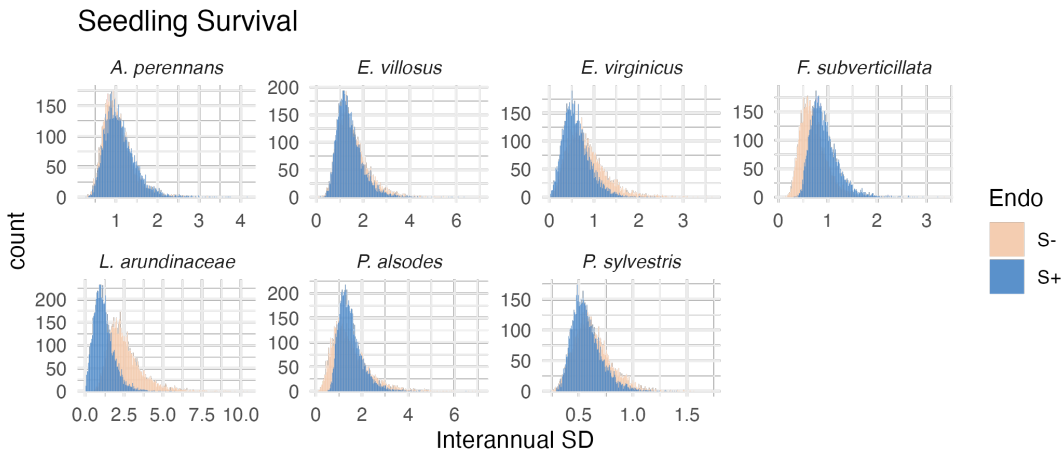


Fig. S12. Posterior distributions of the standard deviations of interannual year effects for seedling survival. Histograms include 7500 post-warmup MCMC samples for symbiotic (S+; blue) and symbiont-free (S-; tan) plants from fitted vital rate model.

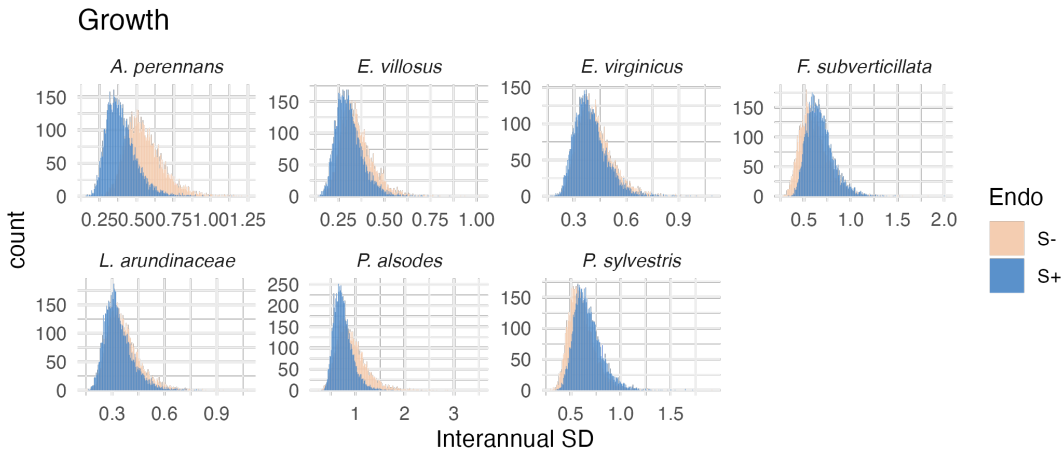


Fig. S13. Posterior distributions of the standard deviations of interannual year effects for growth. Histograms include 7500 post-warmup MCMC samples for symbiotic (S+; blue) and symbiont-free (S-; tan) plants from fitted vital rate model.

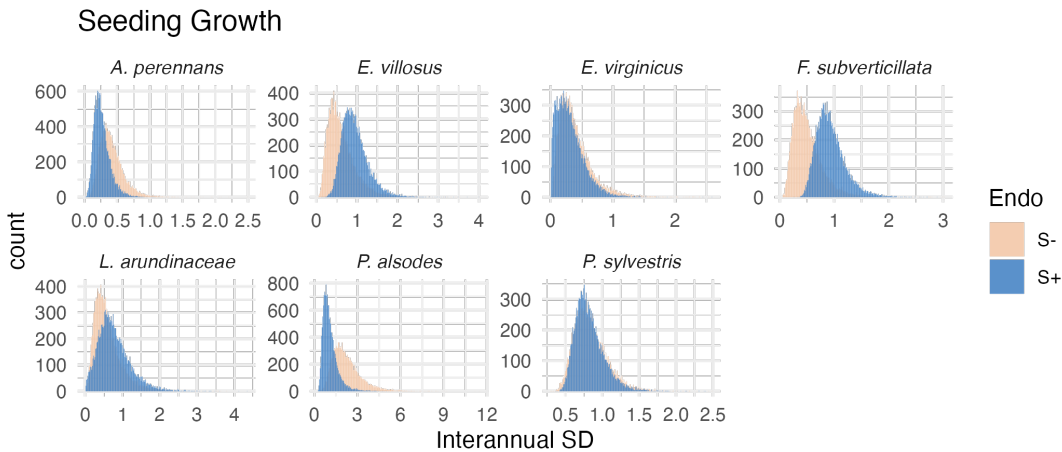


Fig. S14. Posterior distributions of the standard deviations of interannual year effects for seedling growth. Histograms include 7500 post-warmup MCMC samples for symbiotic (S+; blue) and symbiont-free (S-; tan) plants from fitted vital rate model.

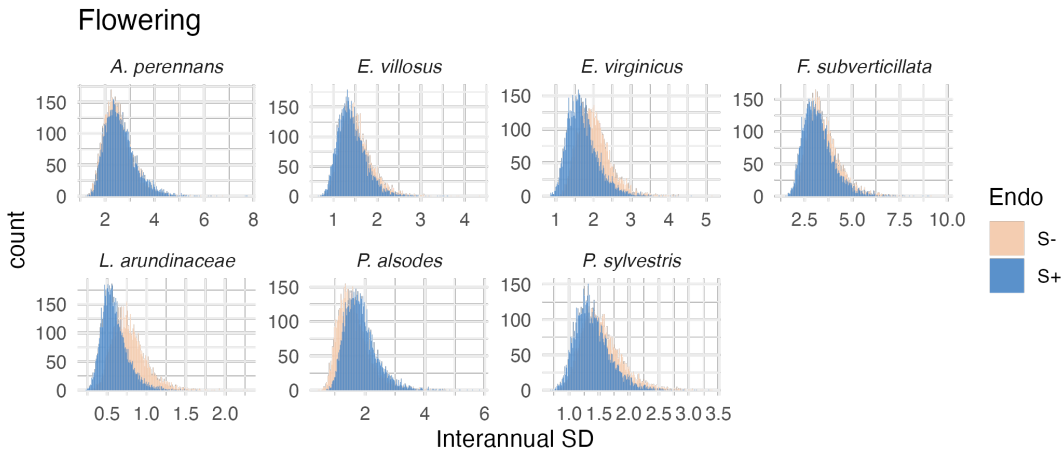


Fig. S15. Posterior distributions of the standard deviations of interannual year effects for flowering probability. Histograms include 7500 post-warmup MCMC samples for symbiotic (S+; blue) and symbiont-free (S-; tan) plants from fitted vital rate model.

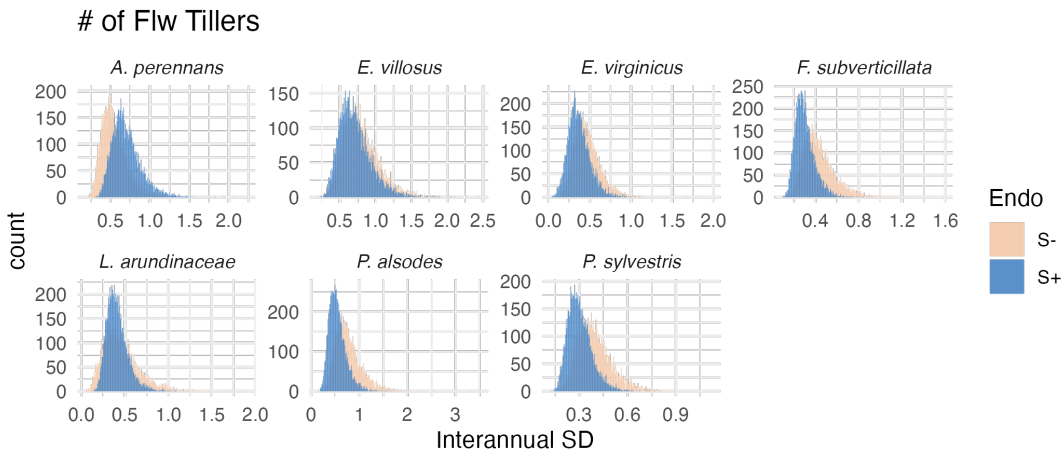


Fig. S16. Posterior distributions of the standard deviations of interannual year effects for fertility (no. of flowering tillers). Histograms include 7500 post-warmup MCMC samples for symbiotic (S+; blue) and symbiont-free (S-; tan) plants from fitted vital rate model.

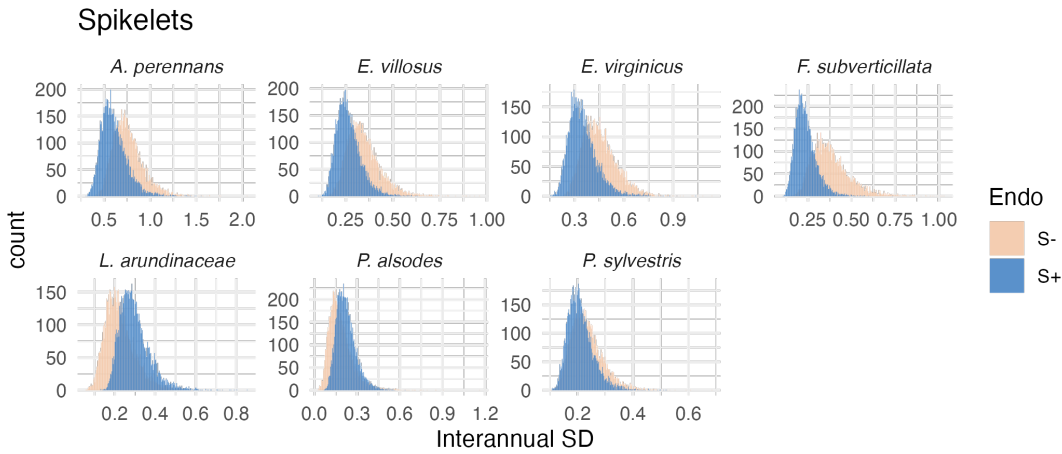


Fig. S17. Posterior distributions of the standard deviations of interannual year effects for spikelets per inflorescence. Histograms include 7500 post-warmup MCMC samples for symbiotic (S+; blue) and symbiont-free (S-; tan) plants from fitted vital rate model.

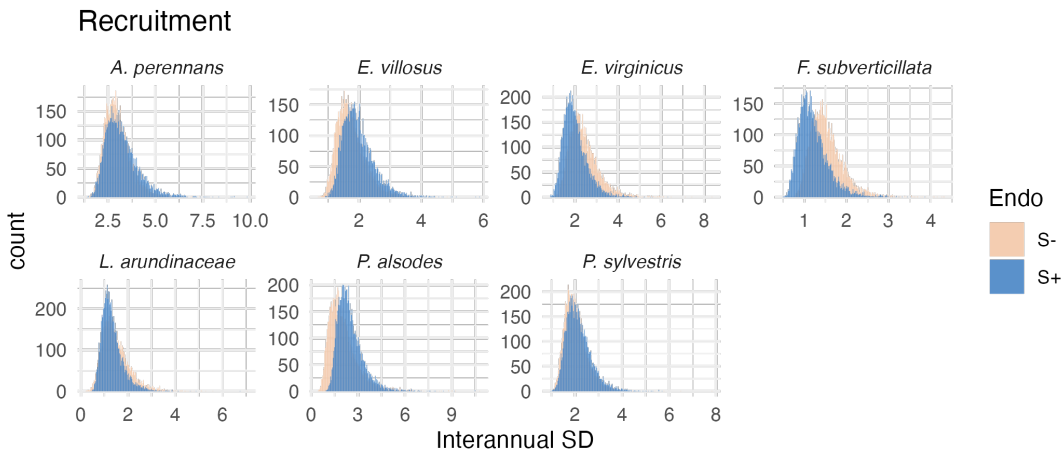


Fig. S18. Posterior distributions of the standard deviations of interannual year effects for recruitment. Histograms include 7500 post-warmup MCMC samples for symbiotic (S+; blue) and symbiont-free (S-; tan) plants from fitted vital rate model.

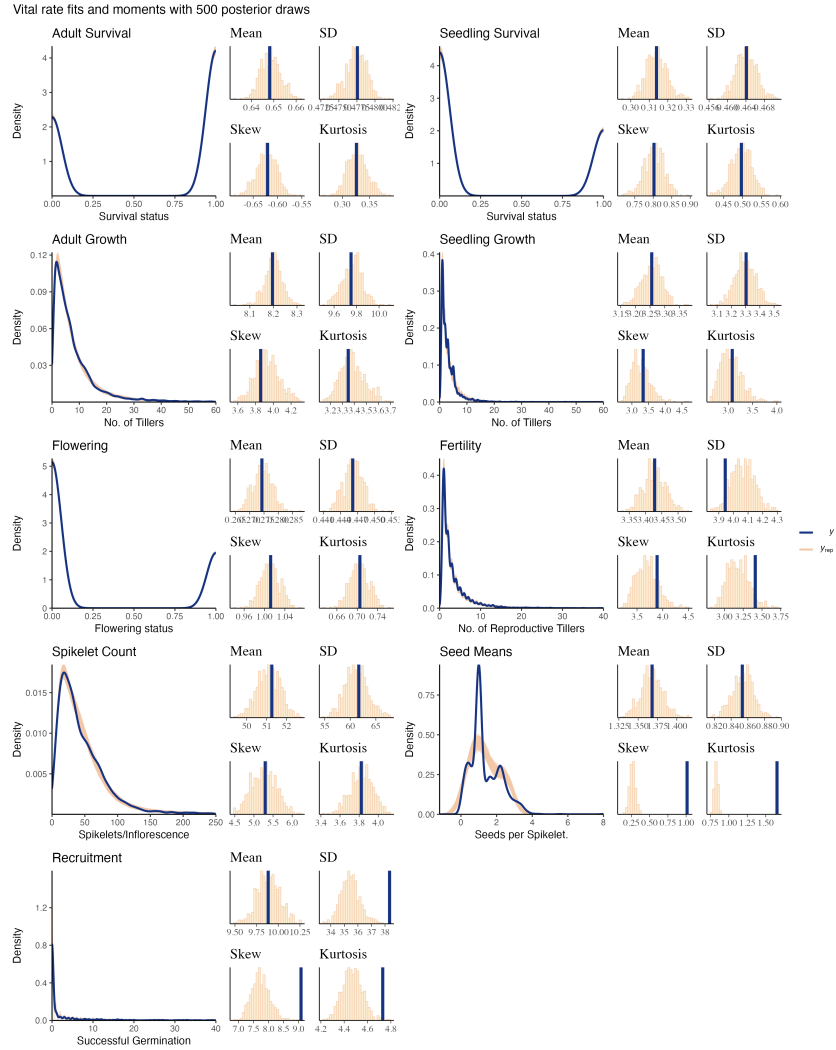


Fig. S19. Consistency between real data and simulated values indicates that fitted models describe the data well. Graphs show posterior predictive check for statistical models of demographic vital rates. Lines show density distributions of observed data (blue line) compared to data simulated from fitted models (tan lines) generated from 500 draws from posterior distributions of model parameters.

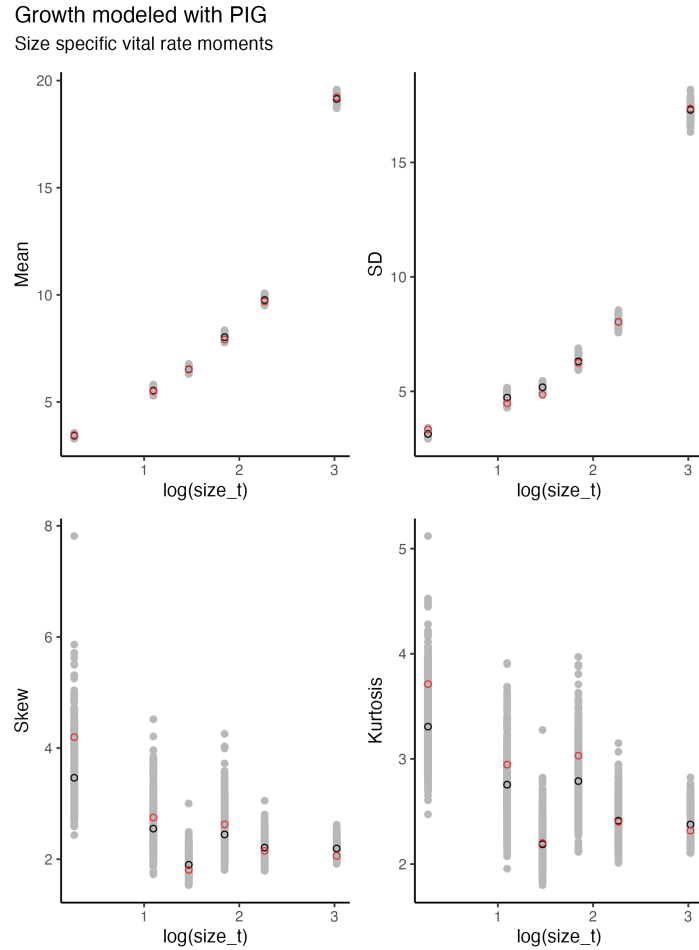


Fig. S20. Consistency between real data and fitted values across sizes indicates that the growth model is accurately capturing size dependence Graphs of posterior predictive check for mean and higher moments of the growth model across size. Points show the value of statistical moments binned across size for the observed data (red circles) compared to the simulated datasets (grey circles) and the median of the simulated values (black circles) generated from 500 posterior draws from the fitted model.

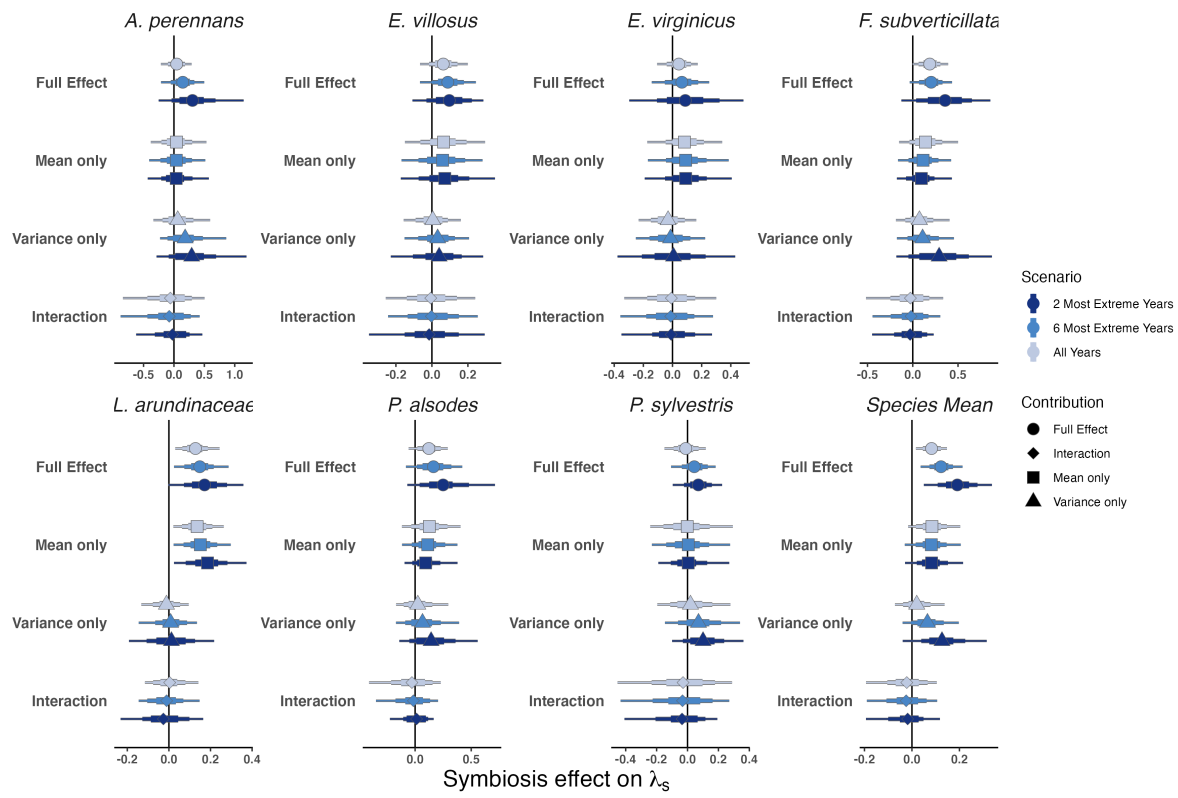


Fig. S21. Endophyte contributions to stochastic growth rates under observed and elevated variance across species. The total effect of endophytes (circle) comes from mean benefits (square) and variance buffering (triangle) as well as the interaction between mean and variance effects (diamond). Shapes indicate the posterior mean of each contribution, along with bars for the 50, 75 and 95 % credible intervals. Under scenarios of increasing variance, represented by increasing color intensity, effects of variance buffering increase leading to a more mutualistic symbiosis.

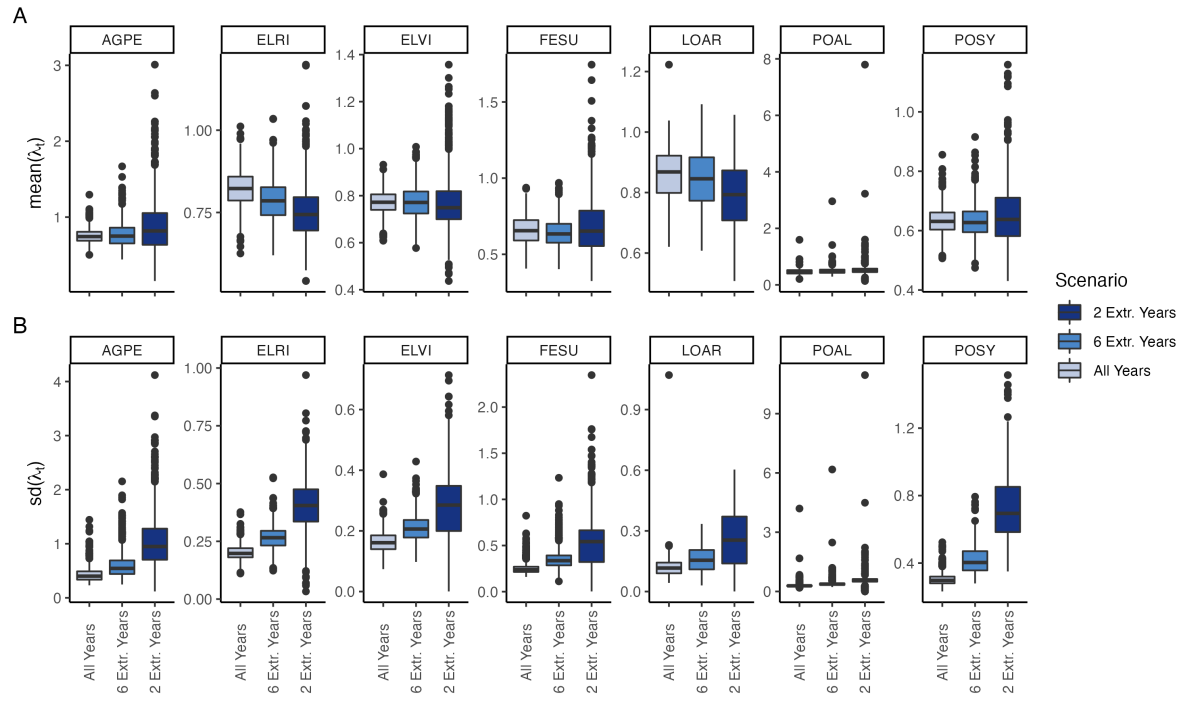


Fig. S22. (A) Mean and (B) standard deviation of annual growth rate values during simulation scenarios. Each scenario selects from observed transition matrixes, increasing the variance by selecting either all observed years, or a set (6 or 2 years) that have the highest and lowest growth rates for symbiont-free populations.

Endophyte Status Checks

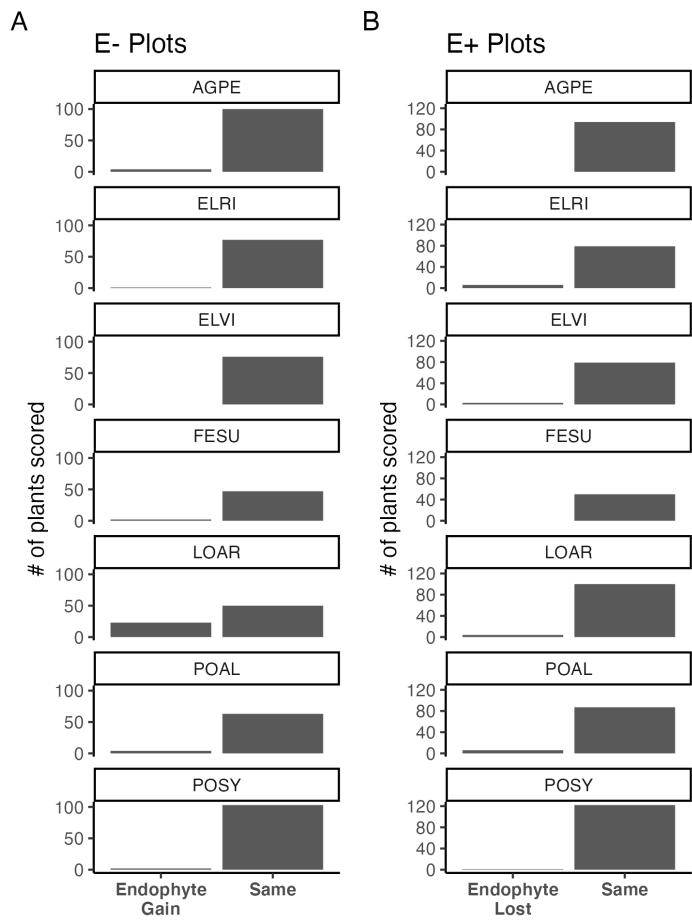


Fig. S23. Faithfulness of experimental plots to assigned endophyte status. Counts of plants scored with leaf peels or seed squashes to check the faithfulness of recruits to the assigned plot-level endophyte status. (A) Endophytic plants may be gained in initially S- plots, or (B) lost in initially S+ plots.

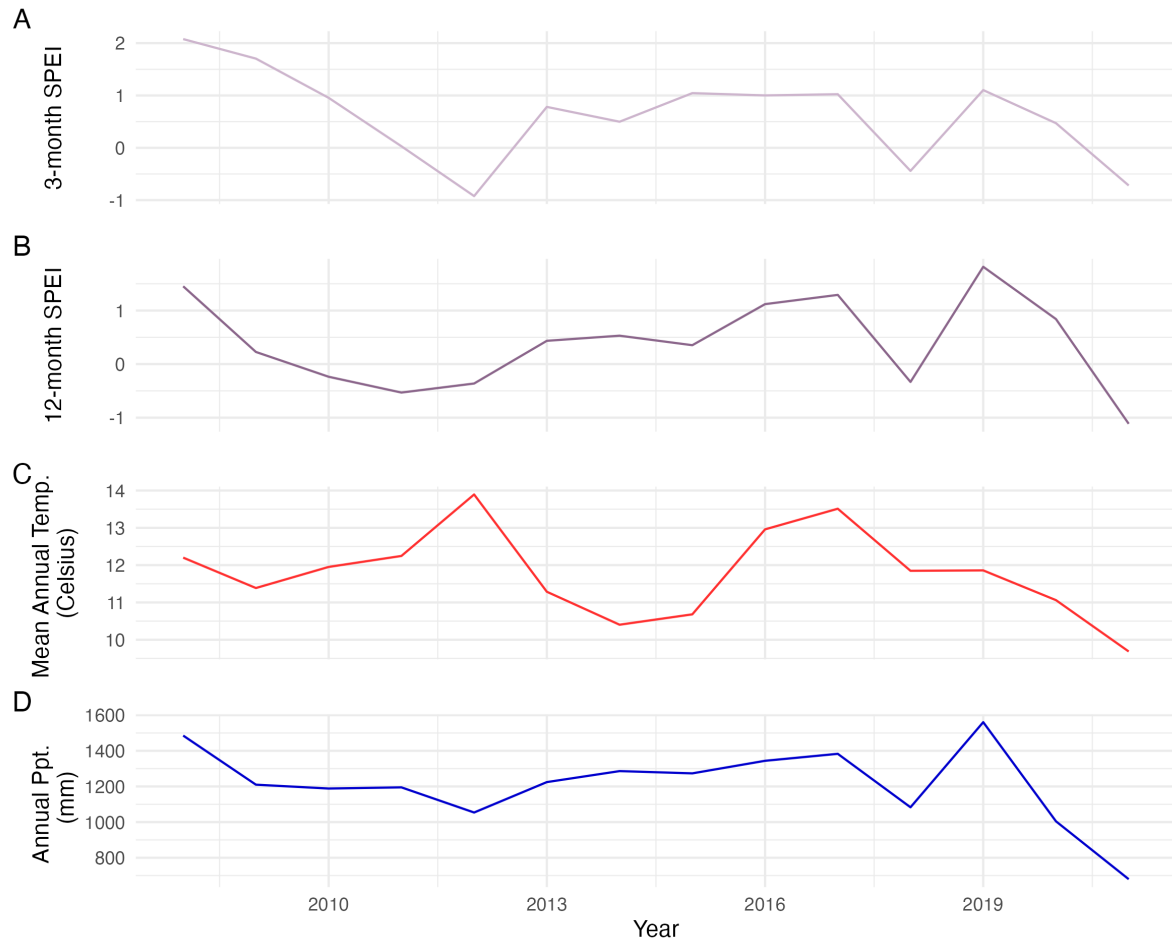


Fig. S24. Weather station time-series for Bloomington, IN. The Seasonal Precipitation-Evapotranspiration Index (SPEI) calculated for the (A) three month growing season and (B) annually from daily weather station observations of (C) average temperatures and (D) cumulative precipitation. Climatic data shown are determined by the census year centered on the month of July.

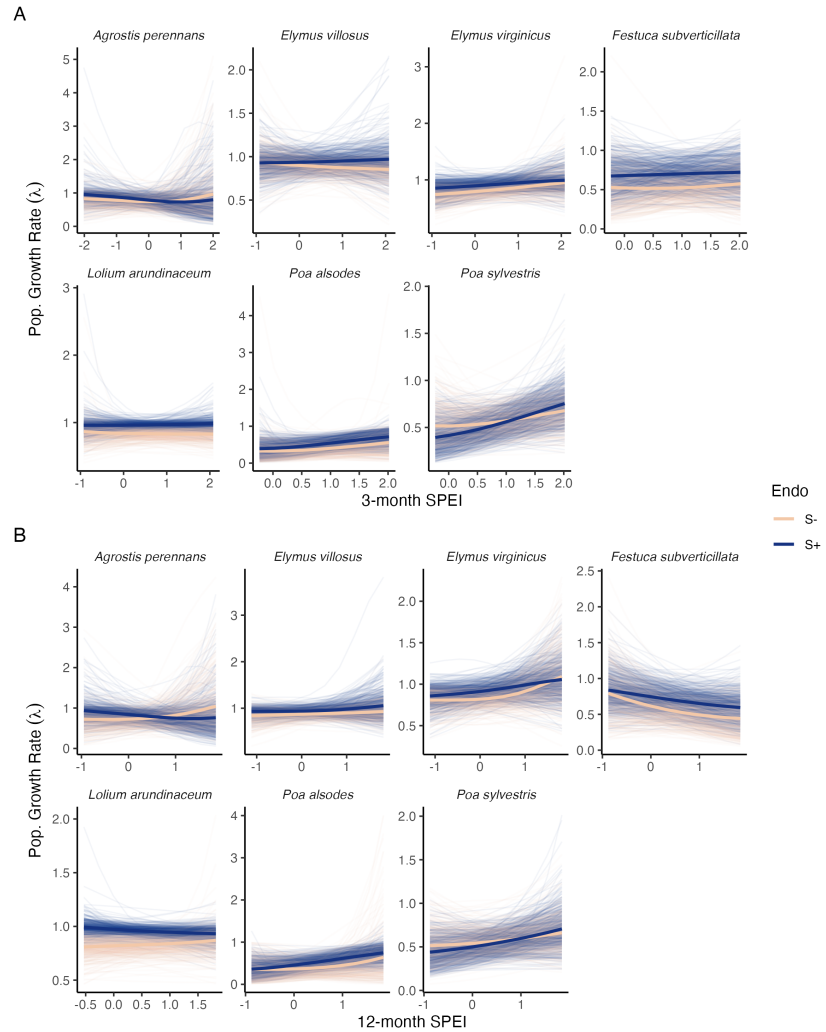


Fig. S25. Predicted population growth rates across drought indices. Symbiotic (S+; blue) and symbiont-free (S-; tan) populations respond differently to climate as measured by the (A) 3-month SPEI and (B) 12-month SPEI. Thick lines represent the predicted mean growth rate and thin lines show 500 posterior draws.

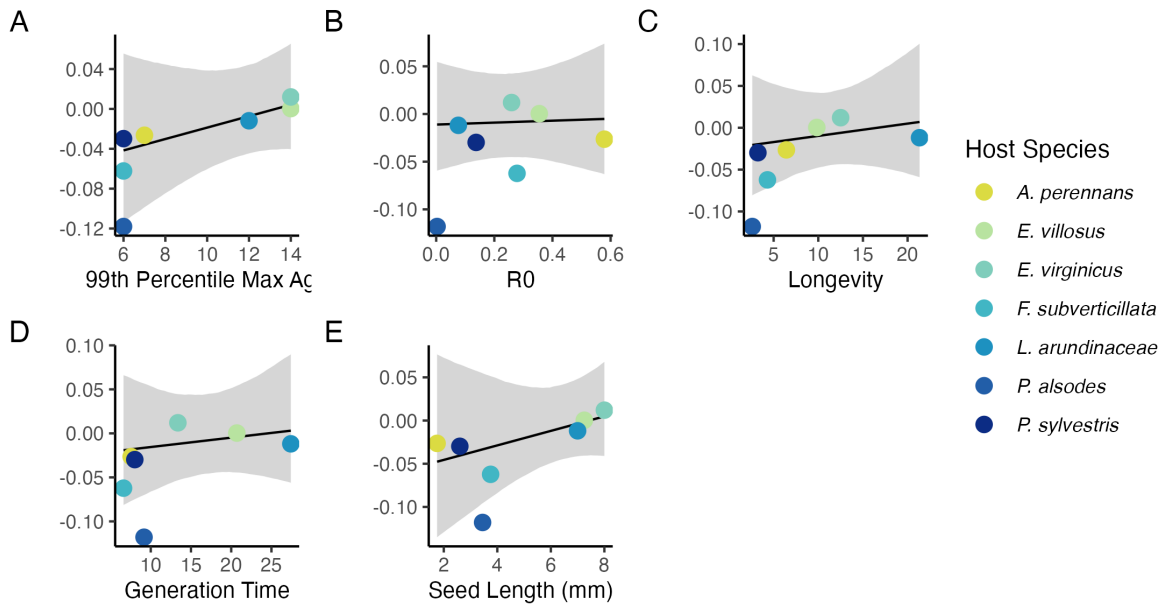


Fig. S26. Relationship between variance buffering and life history traits describing the fast-slow life history continuum accounting for phylogenetic covariance between *Epichloë* symbionts. Results are similar to regressions accounting for host plant phylogeny (Fig. 4), however symbionts are all within a single genus. Each panel shows the fitted mean relationship (line) along with the 95% credible interval.

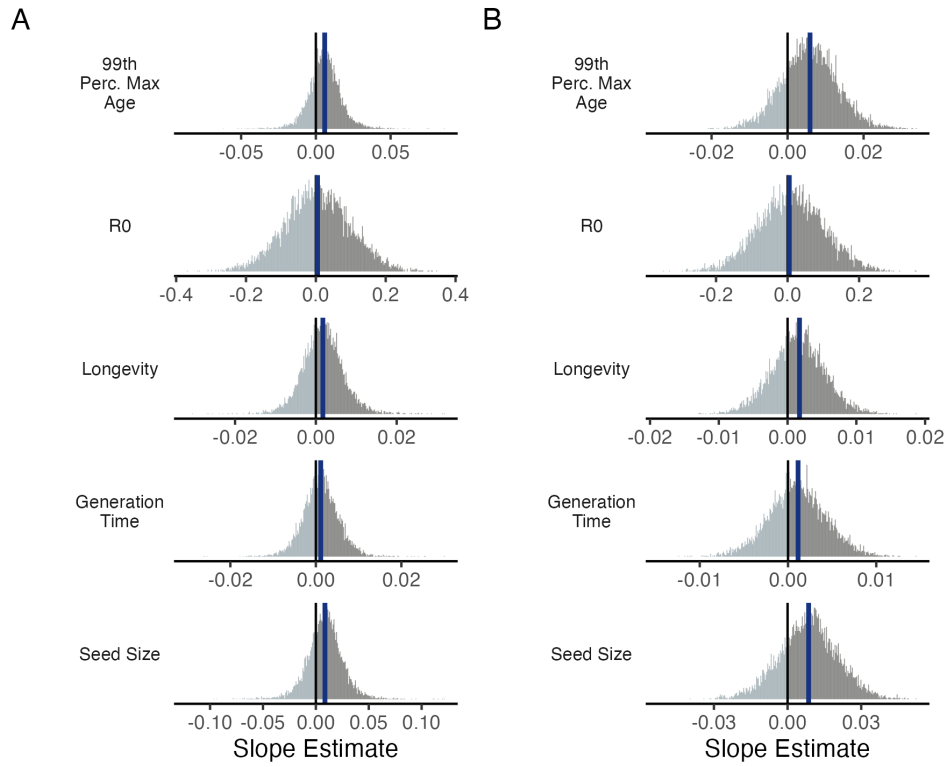


Fig. S27. Posterior estimates of life history trait effects on variance buffering. Grey histograms show the posterior distribution of the slope parameter from models incorporating (A) host plant phylogenetic covariance and (B) symbiont phylogenetic covariance for each life history trait with blue bars showing the posterior mean.

Table S1. Summary of host-endophyte prorogation and transplant methods

Host Species	Symbiont Species	Heat treatment duration (Temp.)	Transplant date
<i>Agrostis perennans</i>	<i>E. amarillans</i>	12 min. hot water bath (60 °C)	April 2008 (10 plots)
<i>Elymus villosus</i>	<i>E. elymi</i>	6 days drying oven (60 °C)	April 2008 (10 plots)
<i>Elymus virginicus</i>	<i>E. elymi or EviTG-1</i>	6 days drying oven (60 °C)	April 2008 (10 plots)
<i>Festuca subverticillata</i>	<i>E. starrii</i>	6 days drying oven (60 °C)	April 2008 (10 plots)
<i>Lolium arundinaceum</i>	<i>E. coenophiala</i>	6 days drying oven (60 °C)	Sept. 2007 (10 plots)
<i>Poa alsodes</i>	<i>E. alsodes</i>	7 days drying oven (60 °C)	Sept. 2007 (8 plots)/April 2008 (10 plots)
<i>Poa sylvestris</i>	<i>E. PsyTG-1</i>	7 days drying oven (60 °C)	Sept. 2007 (8 plots)/April 2008 (10 plots)

Table S2. Summary of focal life history traits

Host Species	Observed max age	99th perc. max age	Generation time	R ₀	Longevity	Seed Length (mm.)	Imperfect transmission rate	Stromata Observed
<i>Agrostis perennans</i>	11	7	7.6	0.58	6.4	1.75	69.8	No
<i>Elymus villosus,</i>	14	14	20.7	0.35	9.8	7.25	100	Yes
<i>Elymus virginicus</i>	14	14	13.4	0.25	12.5	8	100	Yes
<i>Festuca subverticillata</i>	9	6	6.6	0.28	4.3	3.75	42.7	No
<i>Lolium arundinaceum</i>	12*	12*	27.4	0.08	21.3	7	100	No
<i>Poa alsodes</i>	8	6	9.2	0.003	2.6	3.45	99.9	No
<i>Poa sylvestris</i>	12	6	8.0	0.14	3.2	2.6	16.6	Yes

* Censuses for *L. arundinaceum* plots stopped after year 12 of the experiment.

Table S3. Summary of host-endophyte drought sensitivities

Host Species	Effect on CV(λ)	Effect on Mean(λ)	$\frac{\Delta\lambda_{E-}}{\Delta SPEI_3}$	$\frac{\Delta\lambda_{S+}}{\Delta SPEI_3}$	3 month S-to S+ ratio	$\frac{\Delta\lambda_{E-}}{\Delta SPEI_{12}}$	$\frac{\Delta\lambda_{S+}}{\Delta SPEI_{12}}$	12 month S- to S+ ratio
<i>Agrostis perennans</i>	-0.02641	0.04412	0.0341	-0.0400	0.85	0.11410	-0.06255	1.82
<i>Elymus villosus,</i>	0.00033	0.05089	-0.0267	0.0137	1.95	0.02968	0.04216	0.70
<i>Elymus virginicus</i>	0.01201	0.05775	0.0697	0.0465	1.50	0.09677	0.06803	1.42
<i>Festuca subverticillata</i>	-0.06225	0.16393	0.0213	0.0212	1.01	-0.12873	-0.09010	1.43
<i>Lolium arundinaceum</i>	-0.01188	0.10215	-0.0119	0.0090	1.32	0.02644	-0.02596	1.02
<i>Poa alsodes</i>	-0.11798	0.12816	0.1017	0.1429	0.71	0.10457	0.14328	0.73
<i>Poa sylvestris</i>	-0.02981	-0.00852	0.0717	0.1600	0.44	0.05445	0.09820	0.55